

Transverse Single Spin Asymmetry in Open Heavy Flavor Production in Run12 Polarized p+p Collisions at $\sqrt{s} = 200$ GeV

Jeongsu Bok¹, Xiaorong Wang¹, Stephen Pate¹, Vassili Papavassiliou¹,
Haiwang Yu¹, Chen Xu¹, Sanghoon Lim², Ming Liu², Jin Huang³

(1) New Mexico State University

(2) Los Alamos National Laboratory

(3) Brookhaven National Laboratory

January 14, 2017

Contents

1	Introduction	2
2	Run selection	2
3	Event and track selection	3
4	Relative Luminosity	4
5	Single muon measurements	4
6	Transverse single spin asymmetry	5
6.1	Maximum Likelihood Method	5
6.2	Inclusive and background asymmetry estimations	6
6.3	A_N vs. p_T	8
6.3.1	(−) charge	11
6.3.2	(+) charge	15
6.4	A_N vs. x_F	19

6.4.1	(-) charge	19
6.4.2	(+) charge	22
6.5	Systematic uncertainty	25
6.5.1	δf_h Fraction of light hadron background	25
6.5.2	$\delta A_N^{h \rightarrow \mu}$ Difference in Gap3, Gap4 background asymmetry . . .	25
6.5.3	$\delta A_N^{J/\psi \rightarrow \mu}$, Uncertainty in $A_N^{J/\psi \rightarrow \mu}$	27
6.5.4	δA_N^{method} , comparison with cosine fit method	28
7	Simulation to convert theory calculation for A_N of D meson into A_N of muon	35
7.1	converting theory for A_N of D meson into A_N of muon in the kinematic region of this measurement	35
7.2	Additional test with flat A_N input	40
8	results	41
9	Summary	47

Abstract

The transverse single spin asymmetries of single muons from open heavy flavor production in polarized p+p collisions at $\sqrt{s} = 200$ GeV has been analyzed by using run12 data. The run12 recorded luminosity is 9.2 pb^{-1} with average beam polarization about 60%.

1 Introduction

The measurement of transverse single spin asymmetries(A_N) gives us an opportunity to probe the quark and gluon structure of transversely polarized nucleons. Large transverse single spin asymmetries of up to 20% – 40% were discovered for pions produced at large x_F at $\sqrt{s}= 20$ GeV [1, 2] and have been found to persist at RHIC energy $\sqrt{s} = 200$ GeV by the STAR [3] and BRAHMS experiments [4].

At RHIC energy, it is expected that heavy flavor production is dominated by gluon-gluon interaction. Any large transverse single spin asymmetry observed in heavy flavor production cannot originate from the Collins effect because the gluon's transversity is zero. Therefore, the production of heavy flavor particles in transversely polarized p+p collisions at the PHENIX experiment offers a good opportunity to gain information on the gluon's Sivers-type effect. Furthermore, it was shown by M. Anselmino et al. that the single spin asymmetry in open charm production may be significant at forward rapidity which is well covered by the PHENIX muon detectors [5]. So any sizable contributions of A_N in J/ Ψ and open charm production can give a direct measurement of the gluon Sivers-type function.

This analysis has been studied and have a preliminary result of μ^- in Sep 2014[6] with very large(20%) uncertainty in background fraction from AN1174[8]. In 2015, background fraction is finalized by Sanghoon Lim[9], so that we revisited analysis with new background fraction as well as corresponding new cuts.

2 Run selection

In this analysis, the following runs are excluded:

- **Spin information are missing in Spin Database [10]**
358661 358663 358665 358667 359060 359061 359062 359064 362260
- **The spin-pattern polarity swapped midway through the fill [10]**
360473 360474 360475
- **Remove the fills whose polarization for blue beam is not available [10]**
16456
- **Remove the fills whose polarization for yellow beam is not available [10]**
16347 16357 16387 16481 16525 16541

- **Remove runs due to bad mutr QA**
363219 363220
- **Remove low statistics fill 16423**
358924

After all of above QA, 27 runs are excluded, then 340 good runs in 51 fills are used for this analysis. The corresponding effective luminosity can be calculated by

$$\mathcal{L} = N/\sigma_{BBC}, \quad (1)$$

where $\sigma_{BBC} \sim 23$ mb, and $N = N_{EVT-MB} \times \frac{BBCLL1_{live}/BBCLL1_{scaled}}{MuID1D_{live}/MuID1D_{scaled}}$.

3 Event and track selection

Analysis cuts are placed on a track by track basis. The definition of analysis cuts are studied and described as run12 single muon cross section analysis in analysis note 1250 [9]. And this analysis is using the exactly same cuts with those analysis note 1250 used for inclusive single muon candidates. The details are shown below:

- Rapidity cut: $1.4 < |\eta| < 2.0$.
- BBC Vertex Z cut: $-25 < |BBCZ| < 25\text{cm}$.
- p_T range cut: $1.25 < |p_T| < 5\text{GeV}/c$.
- Number of MuTR hits cut: $n\text{MutrHits} \geq 13$.
- MuTR fitting $\chi^2 > 10$ for MUID last gap 2 and 3 , and $\chi^2 > 8$ for last gap 4.

Other cuts :

The DG0, DDG0, VtxRad, VtxChi2, gap0 slope and $|\bar{p} \cdot \delta\theta|$ cuts are used well-studied and fine-tuned transverse momentum dependent cuts from run12 single muon cross section analysis, the cut details are in analysis note 1250[9]. However, we did not apply fiducial 2-D cut in MUTR since this indicates mismatch between simulation and data, while background fraction does not change.

Other cuts used for hadron background (MuID Gap3 tracks): Minimum p_z cut $p_z > 3.4$ was used for removing muons in hadron background.

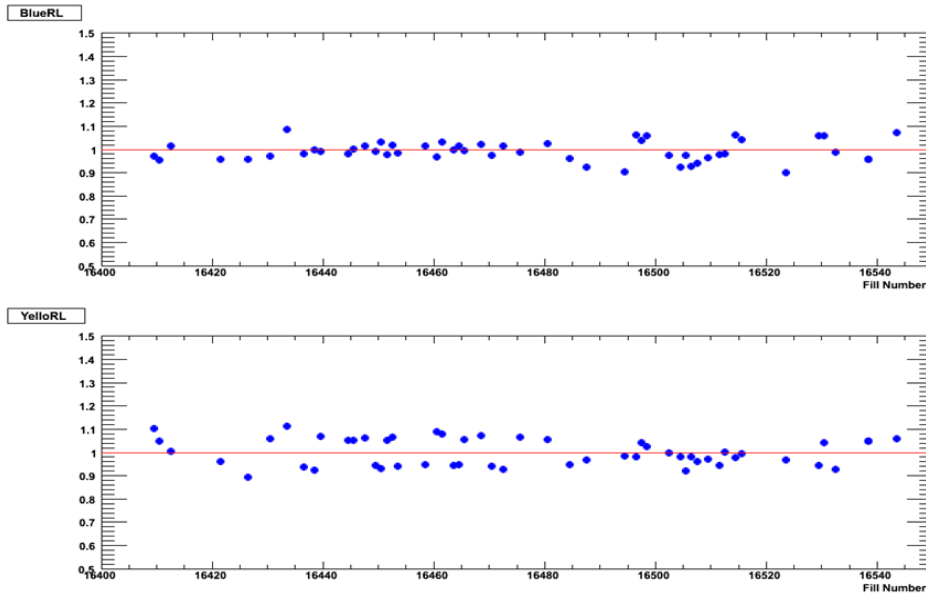


Figure 1: Fill by fill relative luminosity measured by BBCLL1 scaler counts.

4 Relative Luminosity

To obtain the single spin asymmetry, it is essential to know the relative luminosity. In this analysis, we obtained the BBCLL1 counts bunch by bunch from the scaler board called GL1p. Relative luminosity can be calculated by Eq. 2.

$$R_L = \frac{\sum_{bunch} L^\uparrow(bunch)}{\sum_{bunch} L^\downarrow(bunch)} \quad (2)$$

The fill by fill BBCLL1 relative luminosity for Run12 is shown in Figure 1.

5 Single muon measurements

Besides muons from heavy flavor decays, other light hadrons also have finite probability to penetrate the muon spectrometers and be misidentified as a muons. Even worse, since there are no experimental measurements of light hadron yields in the PHENIX muon spectrometers acceptance range, the sources of backgrounds are not well constrained. The dominant sources of backgrounds are:

(1) muons from light hadron decays. Due to the finite distance (40cm) from the collision vertex to the muon spectrometers steel absorber, about 1% of light hadrons decay before they reach the absorber (some of them decay inside the absorber). These decay muons are then measured by the muon spectrometers.

(2) punch-through light hadrons. High momentum light hadrons have finite probability (about < 1%) to reach the last MuID panel and be mis-tagged as muons.

The Run12 single muon cross section analysis has studied the above effects very well, which developed cuts to control the quality of single muon signal and estimated the hadron background fraction. For details about the study, please see AN1250. We applied the identical event and track quality cuts as used in the Run12 single muon cross section analysis for inclusive muons.

6 Transverse single spin asymmetry

The transverse single spin asymmetry A_N is obtained for the blue and yellow beam separately by considering the polarization of only one beam and summing up the polarization of the other beam.

6.1 Maximum Likelihood Method

A detailed discussion on the maximum likelihood method has been made on AN1038. Here, we just simply explain it.

For this measurement, the likelihood is:

$$\zeta = \prod f \cdot (1 \pm R_L \cdot P \cdot A_N \cos(\phi_i)) \quad (3)$$

where f is any correction factor, \pm depends on the spin direction, $R_L = \frac{L^\uparrow}{L^\downarrow}$ is the relative luminosity measured with BBCLL1, P is polarization, ϕ_i is the azimuthal angle for each track. We just look for A_N which would made $\log \zeta$ to reach maximum. Then this A_N will be our result. For some mathematical calculation purpose, the likelihood function is usually written into lg format as:

$$\log \zeta = \sum \log(1 \pm R_L \cdot P \cdot A_N \cos(\phi_i)) + \log f \quad (4)$$

when $\log f$ is independent of A_N , it wouldn't affect the final A_N finding and can be ignored. And if azimuthal angle ϕ distribution didn't have any $\cos()$ modulation, R_L can be ignored too (set to be 1).

The statistical uncertainty can be derived by:

$$\sigma(A_N) = \left(-\frac{\partial^2 \zeta}{\partial A_N^2}\right)^{-1} \quad (5)$$

Since maximum likelihood method doesn't need binning, it is much more reliable than square root formula in low statistics situation.

Because the beam polarization varies fill by fill, the asymmetry is determined fill by fill, then fit to a polynomial of degree 0 across all fills for maximum likelihood method.

6.2 Inclusive and background asymmetry estimations

Tracks at the last MuID gap (Gap4) consist of heavy-flavor muons, punch-through hadrons, muons from light hadrons, and muons from J/ψ . The contribution from other sources is negligible as discussed in the previous section. In order to obtain the asymmetry of heavy-flavor muons (A_N^{HF}), the asymmetry of background from light hadrons (A_N^h) and muons from J/ψ ($A_N^{J/\psi \rightarrow \mu}$) should be subtracted from the asymmetry of inclusive muon candidates (A_N^{incl}). Since hadron tracks can be selected with the p_z cut, the A_N^h is obtained from the asymmetry of stopped hadrons at MuID Gap3. The possible difference between the A_N of the stopped hadron at MuID Gap3 and the mixture of decay muons and punch-through hadrons at MuID Gap4 is studied with the hadron cocktail simulation. The details are described in the following section.

For estimation of $A_N^{J/\psi \rightarrow \mu}$, a previous PHENIX $A_N^{J/\psi}$ measurement [14] is used. The asymmetry of single muons from J/ψ decay ($A_N^{J/\psi \rightarrow \mu}$) is estimated from decay simulation [15] with the initial $A_N^{J/\psi}$ in [14] ($A_N^{J/\psi} = -0.002 \pm 0.026$ in $x_F < 0$, and -0.026 ± 0.026 in $x_F > 0$). The initial p_T and rapidity distributions of J/ψ are from [15]. The obtained $A_N^{J/\psi \rightarrow \mu}$ is $-0.002^{+0.018}_{-0.022}$ in $x_F < 0$ and $-0.019^{+0.019}_{-0.025}$ in $x_F > 0$. Details are in systematic uncertainty section. Once the asymmetries of light hadron background (A_N^h) and muons from J/ψ ($A_N^{J/\psi \rightarrow \mu}$) are determined, the A_N of heavy-flavor muons and its uncertainty can be obtained as

$$A_N^{HF} = \frac{A_N^{incl} - f_h \cdot A_N^h - f_{J/\psi} \cdot A_N^{J/\psi \rightarrow \mu}}{1 - f_h - f_{J/\psi}}, \quad (6)$$

$$\delta A_N^{HF} = \frac{\sqrt{(\delta A_N^{incl})^2 + f_h^2 \cdot (\delta A_N^h)^2 + f_{J/\psi}^2 \cdot (\delta A_N^{J/\psi \rightarrow \mu})^2}}{1 - f_h - f_{J/\psi}}, \quad (7)$$

where $f_h = (N_{DM} + N_{PH})/N_{incl}$ is the fraction of light hadron background, and $f_{J/\psi} = N_{J/\psi \rightarrow \mu}/N_{incl}$ is the fraction of muons from J/ψ . Both fractions (f_h and $f_{J/\psi}$) are determined from the background estimation. $\delta A_N^{J/\psi \rightarrow \mu}$ estimated with the previous PHENIX measurement is included only in systematic uncertainty.

Table 1: The light hadron background fraction (f_h) in p_T bins, (-)charge

p_T GeV/c	South Arm			North Arm		
	f_h	δf_h^{syst}	δf_h^{stat}	f_h	δf_h^{syst}	δf_h^{stat}
(1.25,1.50)	78.15%	10.52%	0.41%	78.62%	9.35%	0.41%
(1.50,2.00)	76.88%	10.28%	0.40%	75.06%	8.72%	0.37%
(2.00,2.50)	70.36%	9.41%	0.66%	72.65%	8.36%	0.62%
(2.50,3.00)	59.10%	7.78%	0.96%	59.98%	6.80%	0.89%
(3.00,3.50)	50.06%	6.89%	1.39%	52.09%	5.17%	1.51%
(3.50,5.00)	46.11%	7.38%	1.67%	46.16%	6.03%	1.51%

Table 2: The background fraction (f_h) in x_F bins, (-)charge

$ x_F $	South Arm			North Arm		
	f_h	δf_h^{syst}	δf_h^{stat}	f_h	δf_h^{syst}	δf_h^{stat}
(0.00,0.05)	77.74%	10.46%	0.31%	77.78%	9.25%	0.30%
(0.05,0.20)	70.84%	9.47%	0.49%	69.23%	7.97%	0.44%

Table 1, 2, 3, and 4 list the light hadron background fraction we calculate from the signal to (light hadron) background ratio from Run12 p+p single muon cross section analysis [9]. We will use these ratios to calculate our physics asymmetries. Systematic Uncertainty of light hadron background fraction was used as a source of systematic uncertainty. Table 5,jpsi-fraction-pt-plus,jpsi-fraction-xf represent the J/ψ fraction. It was calculated in PHENIX analysis note [15]. $N_{HF+J/\psi}$ means the number of heavy flavor including J/ψ , only light hadron background is subtracted from inclusive tracks

Table 3: The background fraction (r) in p_T bins, (+)charge

p_T GeV/c	South Arm			North Arm		
	f_h	δf_h^{syst}	δf_h^{stat}	f_h	δf_h^{syst}	δf_h^{stat}
(1.25,1.50)	78.17%	10.69%	0.41%	83.49%	10.60%	0.46%
(1.50,2.00)	73.03%	9.76%	0.37%	77.65%	9.15%	0.37%
(2.00,2.50)	70.97%	9.30%	0.60%	72.71%	8.14%	0.58%
(2.50,3.00)	64.97%	8.46%	0.93%	64.07%	7.07%	0.90%
(3.00,3.50)	59.21%	9.58%	1.40%	57.89%	6.78%	1.29%
(3.50,5.00)	60.23%	8.84%	1.80%	55.26%	6.27%	1.56%

Table 4: The background fraction (r) in x_F bins, (+)charge

$ x_F $	South Arm			North Arm		
	f_h	δf_h^{syst}	δf_h^{stat}	f_h	δf_h^{syst}	δf_h^{stat}
(0.00,0.05)	76.57%	10.47%	0.30%	81.57%	10.36%	0.33%
(0.05,0.20)	70.18%	9.20%	0.44%	72.06%	8.06%	0.45%

Table 5: J/ψ fraction in p_T bins, (-)charge

p_T GeV/c	South Arm		North Arm	
	$N_{J/\psi}/N_{HF+J/\psi}$	$f_{J/\psi}$ (absolute)	$N_{J/\psi}/N_{HF}$	$f_{J/\psi}$ (absolute)
(1.25,1.50)	1.83%	0.40%	2.13%	0.46%
(1.50,2.00)	4.76%	1.10%	4.90%	1.22%
(2.00,2.50)	11.15%	3.30%	13.25%	3.62%
(2.50,3.00)	14.64%	5.99%	16.11%	6.45%
(3.00,3.50)	16.75%	8.36%	18.58%	8.90%
(3.50,5.00)	20.36%	10.97%	22.30%	12.01%

6.3 A_N vs. p_T

The transverse single spin asymmetry in μ^- and μ^+ production have been studied in six p_T ($1.25 < p_T < 5$ GeV/c) bins for forward and backward rapidity separately.

Table 6: J/ψ fraction in p_T bins, (+)charge

p_T GeV/c	South Arm		North Arm	
	$N_{J/\psi}/N_{HF}$	$f_{J/\psi}$ (absolute)	$N_{J/\psi}/N_{HF+J/\psi}$	$f_{J/\psi}$ (absolute)
(1.25,1.50)	1.49%	0.32%	2.30%	0.38%
(1.50,2.00)	3.30%	0.89%	4.51%	1.01%
(2.00,2.50)	9.00%	2.61%	10.44%	2.85%
(2.50,3.00)	13.00%	4.55%	13.50%	4.85%
(3.00,3.50)	14.62%	5.96%	15.72%	6.62%
(3.50,5.00)	18.34%	7.29%	18.46%	8.26%

Table 7: J/ψ fraction in x_F bins, (-)charge

$ x_F $	South Arm		North Arm	
	$N_{J/\psi}/N_{HF+J/\psi}$	$f_{J/\psi}$ (absolute)	$N_{J/\psi}/N_{HF+J/\psi}$	$f_{J/\psi}$ (absolute)
(0.00,0.05)	5.11%	1.14%	5.69%	1.26%
(0.05,0.20)	16.74%	4.88%	18.51%	5.69%

Table 8: J/ψ fraction in x_F bins, (+)charge

$ x_F $	South Arm		North Arm	
	$N_{J/\psi}/N_{HF+J/\psi}$	$f_{J/\psi}$ (absolute)	$N_{J/\psi}/N_{HF+J/\psi}$	$f_{J/\psi}$ (absolute)
(0.00,0.05)	3.88%	0.91%	5.00%	0.92%
(0.05,0.20)	14.79%	4.41%	15.36%	4.29%

To have a rough idea of the statistics, the tracks for inclusive muons (Gap4) and hadron background(Gap3) after all the quality cuts is listed in table 9,10.

Table 9: Number of $(-)$ tracks in different Gaps after all the track quality cuts.

p_T	N(South, Gap3)	N(South, Gap4)	N(North, Gap3)	N(North, Gap4)
(1.25, 5.0)	32476	588964	30545	624773
(1.25, 1.5)	7750	274922	6697	264517
(1.5, 2.0)	13295	234272	12511	267715
(2.0, 2.5)	6332	55908	6238	65152
(2.5, 3.0)	2858	16181	2802	18444
(3.0, 3.5)	1241	4819	1273	5958
(3.5, 5.0)	1000	2862	1024	2987

Table 10: Number of $(+)$ tracks in different Gaps after all the track quality cuts.

p_T	N(South, Gap3)	N(South, Gap4)	N(North, Gap3)	N(North, Gap4)
(1.25, 5.0)	75195	682849	71610	298184
(1.25, 1.5)	18365	314778	15106	298184
(1.5, 2.0)	30942	270782	29372	304978
(2.0, 2.5)	14555	66768	15046	78534
(2.5, 3.0)	6431	20116	6788	23509
(3.0, 3.5)	2695	6285	2988	8026
(3.5, 5.0)	2207	4120	2399	4312

6.3.1 (-) charge

Figure 2, 3 and 4 show the p_T dependence of asymmetries in single track production at Gap4 (inclusive asymmetries), Gap3 (background asymmetries) and physics asymmetries respectively. Since our p_T range of single muons is from $1.25 < p_T < 5\text{GeV}/c$, within the limits of errors, the asymmetry for Gap3 muons (mainly from light hadron) are consistent with zero for all p_T bins as expected from the previous experimental results. The asymmetries (blue beam, yellow beam and combined) at forward rapidity for Gap3 (background) and Gap4 (inclusive) are listed in table 11.

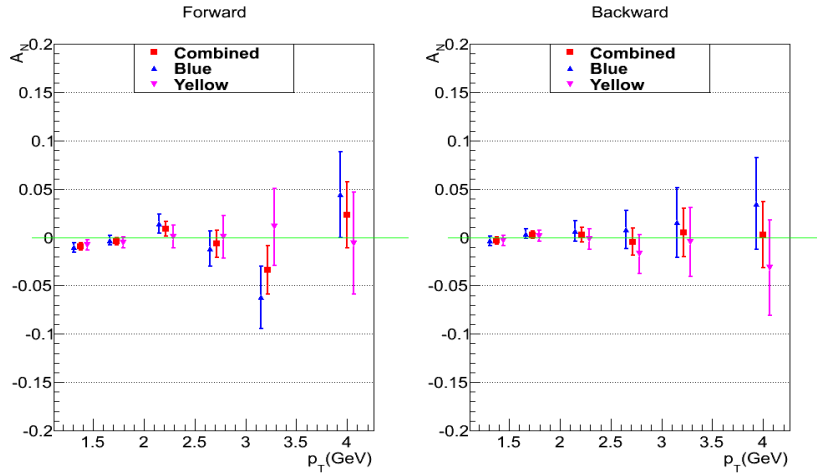


Figure 2: p_T dependence of asymmetries for inclusive muons (Gap4) in the forward (left) and backward (right) rapidity. (-)charge

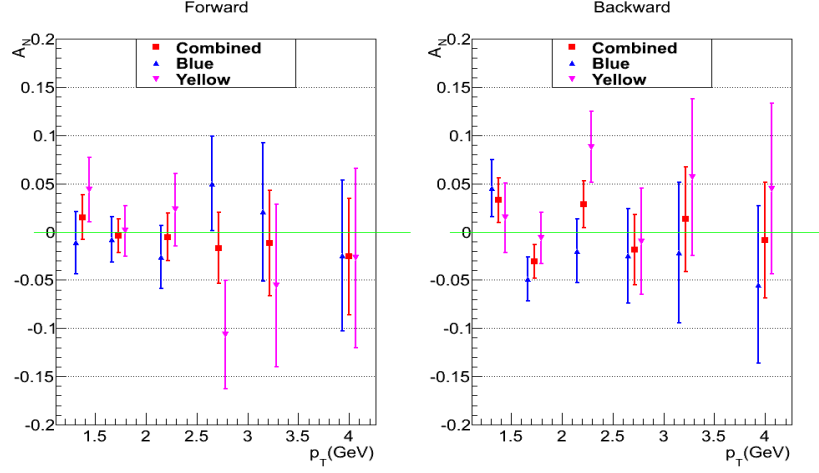


Figure 3: p_T dependence of asymmetries for hadrons background (Gap3) in the forward (left) and backward (right) rapidity. (-)charge

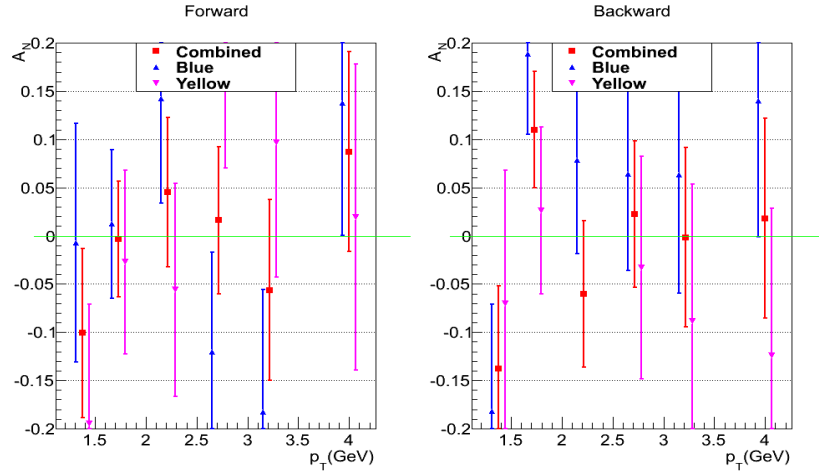


Figure 4: p_T dependence of physics asymmetries in the forward (left) and backward (right) rapidity, which were obtained by using formula (6) and (7) with $A_N(\text{Inclusive})= A_N(\text{Gap4})$ and $A_N(\text{Background})=A_N(\text{Gap3})$. (-)charge

Table 11: p_T dependence of A_N^B (Blue Beam), A_N^Y (Yellow Beam) and A_N (Combined) in forward rapidity. (-)charge

p_T (GeV)	Gap4 (10^{-2})			Gap3 (10^{-2})		
	A_N^B	A_N^Y	A_N	A_N^B	A_N^Y	A_N
(1.25,1.50)	-1.05±0.49	-0.81±0.54	-0.94±0.36	-1.13±3.23	4.33±3.34	1.51±2.32
(1.50,2.00)	-0.31±0.48	-0.55±0.58	-0.41±0.37	-0.77±2.34	0.09±2.62	-0.39±1.75
(2.00,2.50)	1.39±0.98	0.07±1.19	0.86±0.76	-2.63±3.26	2.29±3.78	-0.53±2.47
(2.50,3.00)	-1.15±1.83	0.05±2.21	-0.66±1.41	5.01±4.88	-10.65±5.63	-1.70±3.69
(3.00,3.50)	-6.21±3.21	1.07±4.00	-3.35±2.50	2.05±7.21	-5.59±8.42	-1.18±5.48
(3.50,5.00)	4.41±4.47	-0.63±5.28	2.31±3.41	-2.47±7.84	-2.73±9.33	-2.58±6.00

Table 12: p_T dependence of A_N^B (Blue Beam), A_N^Y (Yellow Beam) and A_N (Combined) in backward rapidity. (-)charge

p_T (GeV)	Gap4 (10^{-2})			Gap3 (10^{-2})		
	A_N^B	A_N^Y	A_N	A_N^B	A_N^Y	A_N
(1.25,1.50)	-0.37±0.49	-0.33±0.55	-0.35±0.36	4.51±2.97	1.45±3.61	3.27±2.29
(1.50,2.00)	0.37±0.52	0.15±0.53	0.26±0.37	-4.91±2.29	-0.63±2.64	-3.07±1.73
(2.00,2.50)	0.67±1.06	-0.19±1.08	0.25±0.76	-1.99±3.31	8.79±3.67	2.85±2.46
(2.50,3.00)	0.77±1.98	-1.73±2.02	-0.46±1.41	-2.49±4.88	-1.01±5.52	-1.84±3.66
(3.00,3.50)	1.53±3.58	-0.51±3.56	0.50±2.52	-2.17±7.29	5.65±8.13	1.32±5.43
(3.50,5.00)	3.47±4.76	-3.15±4.91	0.27±3.42	-5.47±8.17	4.47±8.85	-0.89±6.00

Table 13: p_T dependence of physics A_N^B (Blue Beam), A_N^Y (Yellow Beam) and A_N (Combined). The physics asymmetries were obtained by using formula (6) and (7) with A_N (Inclusive)= A_N (Gap4) and A_N (Background)= A_N (Gap3). (-)charge

p_T (GeV)	Forward (10^{-2})			Backward (10^{-2})		
	A_N^B	A_N^Y	A_N	A_N^B	A_N^Y	A_N
(1.25,1.50)	-0.73±12.36	-19.51±12.43	-10.07±8.76	-18.15±11.05	-7.02±13.80	-13.80±8.63
(1.50,2.00)	1.23±7.69	-2.72±9.52	-0.33±5.98	18.83±8.35	2.64±8.64	11.01±6.01
(2.00,2.50)	14.20±10.80	-5.61±11.07	4.54±7.73	7.88±9.72	-27.68±12.12	-6.05±7.58
(2.50,3.00)	-12.01±10.28	18.50±11.46	1.60±7.65	6.45±10.03	-3.32±11.54	2.25±7.57
(3.00,3.50)	-18.22±12.67	9.69±13.97	-5.63±9.38	6.33±12.31	-8.81±14.18	-0.18±9.29
(3.50,5.00)	13.81±13.74	1.95±15.86	8.73±10.39	14.01±14.14	-12.41±15.27	1.81±10.38

6.3.2 (+) charge

The asymmetries (blue beam, yellow beam and combined) at backward rapidity for Gap3 (background) and Gap4 (inclusive) are listed in table 15. And the physics asymmetries listed in the table 16 were calculated by using the formula (6), (7) and table 3. The asymmetries (blue beam, yellow beam and combined) at forward rapidity for Gap3 (background) and Gap4 (inclusive) are listed in table 11.

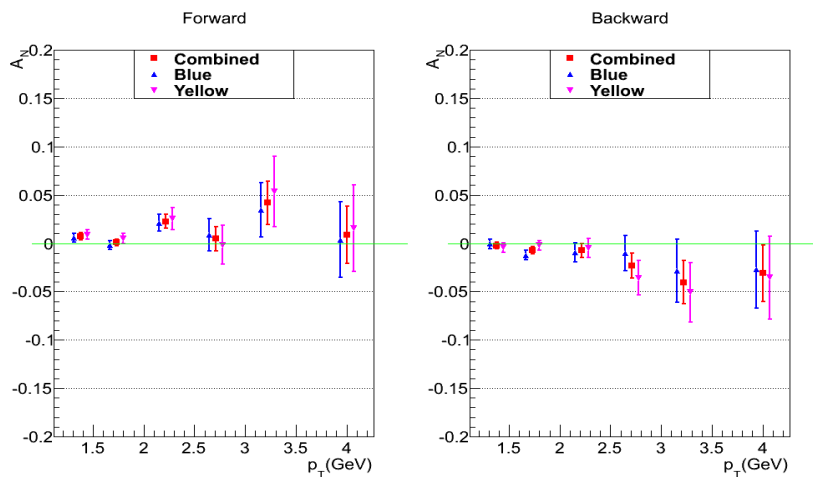


Figure 5: p_T dependence of asymmetries for inclusive muons (Gap4) in the forward (left) and backward (right) rapidity. (+)charge

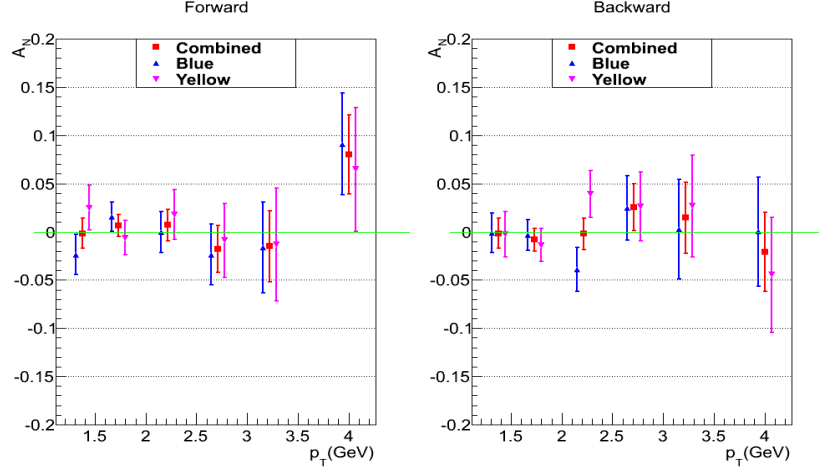


Figure 6: p_T dependence of asymmetries for hadrons background (Gap3) in the forward (left) and backward (right) rapidity. (+)charge

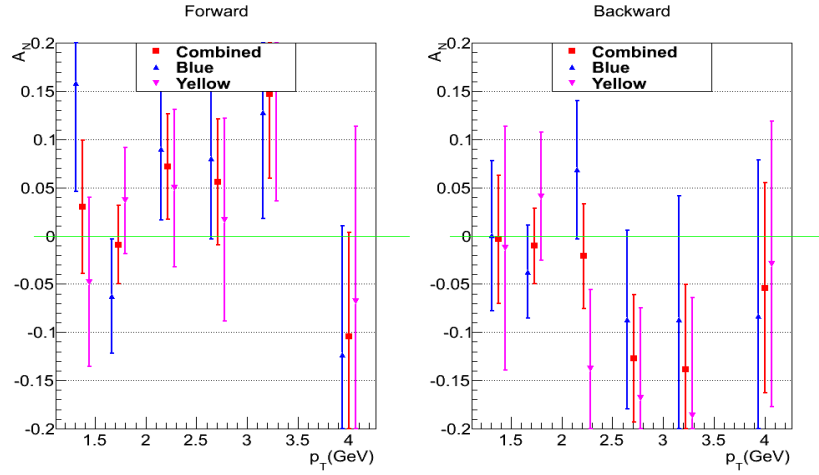


Figure 7: p_T dependence of physics asymmetries in the forward (left) and backward (right) rapidity, which were obtained by using formula (6) and (7) with $A_N(\text{Inclusive})= A_N(\text{Gap4})$ and $A_N(\text{Background})=A_N(\text{Gap3})$. (+)charge

Table 14: p_T dependence of A_N^B (Blue Beam), A_N^Y (Yellow Beam) and A_N (Combined) in forward rapidity. (+)charge

p_T (GeV)	Gap4 (10^{-2})			Gap3 (10^{-2})		
	A_N^B	A_N^Y	A_N	A_N^B	A_N^Y	A_N
(1.25,1.50)	0.57±0.47	0.91±0.53	0.72±0.35	-2.37±2.11	2.49±2.32	-0.17±1.56
(1.50,2.00)	-0.17±0.46	0.49±0.56	0.09±0.35	1.53±1.52	-0.61±1.80	0.64±1.16
(2.00,2.50)	2.11±0.90	2.53±1.12	2.27±0.70	-0.05±2.14	1.79±2.60	0.69±1.65
(2.50,3.00)	0.87±1.64	-0.17±2.03	0.46±1.27	-2.39±3.15	-0.91±3.80	-1.79±2.43
(3.00,3.50)	3.47±2.81	5.37±3.64	4.18±2.22	-1.63±4.69	-1.33±5.84	-1.51±3.66
(3.50,5.00)	0.37±3.90	1.55±4.45	0.88±2.93	9.11±5.31	6.47±6.43	8.04±4.10

Table 15: p_T dependence of A_N^B (Blue Beam), A_N^Y (Yellow Beam) and A_N (Combined) in backward rapidity. (+)charge

p_T (GeV)	Gap4 (10^{-2})			Gap3 (10^{-2})		
	A_N^B	A_N^Y	A_N	A_N^B	A_N^Y	A_N
(1.25,1.50)	-0.07±0.48	-0.45±0.51	-0.25±0.35	-0.09±2.06	-0.29±2.36	-0.18±1.55
(1.50,2.00)	-1.23±0.50	-0.21±0.50	-0.72±0.36	-0.35±1.58	-1.39±1.71	-0.83±1.16
(2.00,2.50)	-0.97±1.00	-0.53±0.99	-0.75±0.70	-3.91±2.28	3.91±2.40	-0.21±1.65
(2.50,3.00)	-1.05±1.82	-3.57±1.81	-2.32±1.28	2.47±3.33	2.61±3.57	2.53±2.43
(3.00,3.50)	-2.87±3.25	-5.07±3.09	-4.03±2.24	0.27±5.14	2.69±5.28	1.45±3.68
(3.50,5.00)	-2.71±4.00	-3.55±4.28	-3.10±2.92	0.01±5.63	-4.47±5.97	-2.10±4.10

Table 16: p_T dependence of physics A_N^B (Blue Beam), A_N^Y (Yellow Beam) and A_N (Combined). The physics asymmetries were obtained by using formula (6) and (7) with A_N (Inclusive)= A_N (Gap4) and A_N (Background)= A_N (Gap3). (+)charge

p_T (GeV)	Forward (10^{-2})			Backward (10^{-2})		
	A_N^B	A_N^Y	A_N	A_N^B	A_N^Y	A_N
(1.25,1.50)	15.84±11.29	-4.79±8.78	2.99±6.93	0.00±7.80	-1.28±12.61	-0.35±6.63
(1.50,2.00)	-6.28±5.94	3.65±5.49	-0.92±4.03	-3.73±4.84	4.08±6.65	-1.03±3.91
(2.00,2.50)	9.00±7.34	4.96±8.17	7.20±5.46	6.85±7.20	-13.78±8.22	-2.10±5.41
(2.50,3.00)	8.02±8.36	1.67±10.49	5.55±6.54	-8.69±9.27	-16.84±9.39	-12.71±6.60
(3.00,3.50)	12.79±11.00	18.01±14.41	14.71±8.74	-8.67±12.79	-18.64±12.25	-13.87±8.85
(3.50,5.00)	-12.36±13.38	-6.80±18.17	-10.40±10.77	-8.32±16.15	-2.92±14.82	-5.39±10.92

6.4 A_N vs. x_F

The single spin asymmetry has also been studied in four x_F ($-0.2 < x_F < 0.2$) bins. Figure 8, 9 and 10(for $(-)$ charge), Figure 11, 12 and 13(for $(+)$ charge), shows the x_F dependence of asymmetries at Gap4(inclusive asymmetries), Gap3(background asymmetries) and physics asymmetries respectively. The physics asymmetries listed in table 17($(-)$ charge) and 19($(+)$ charge) were calculated by using the formula (6), (7) and table 2.

6.4.1 $(-)$ charge

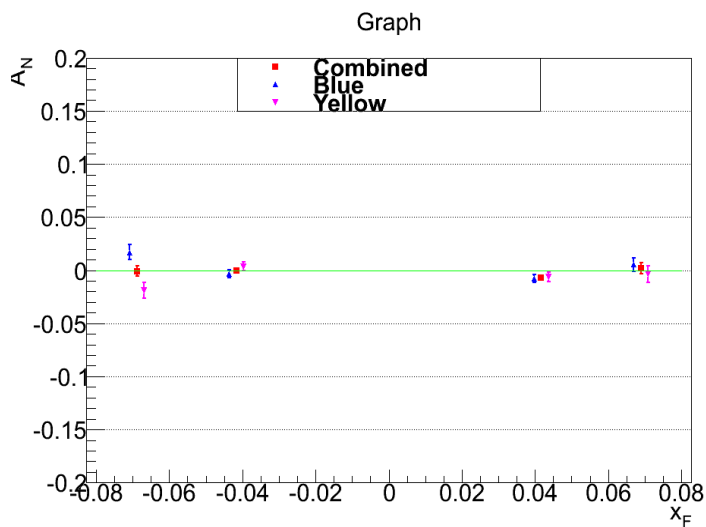


Figure 8: x_F dependence of asymmetries for inclusive muons (Gap4). $(-)$ charge

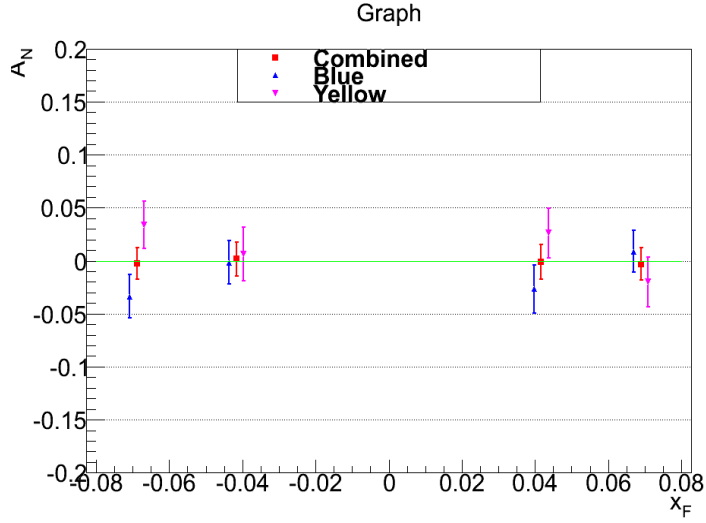


Figure 9: x_F dependence of asymmetries for hadron background (Gap3). (-)charge

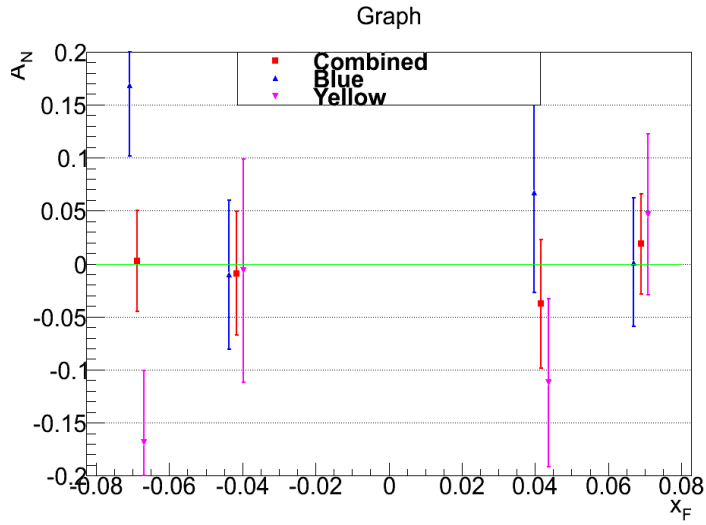


Figure 10: x_F dependence of physics asymmetries, which were obtained by using formula (6) and (7) with $A_N(\text{Inclusive}) = A_N(\text{Gap4})$ and $A_N(\text{Background}) = A_N(\text{Gap23})$. (-)charge

Table 17: x_F dependence of A_N^B (Blue Beam), A_N^Y (Yellow Beam) and A_N (Combined). (-)charge

x_F	Gap4 (10^{-2})			Gap3 (10^{-2})		
	A_N^B	A_N^Y	A_N	A_N^B	A_N^Y	A_N
(-0.20,-0.05)	1.71 ± 0.72	-1.89 ± 0.72	-0.08 ± 0.51	-3.35 ± 2.05	3.41 ± 2.23	-0.25 ± 1.51
(-0.05,0.00)	-0.35 ± 0.37	0.37 ± 0.40	-0.02 ± 0.27	-0.15 ± 2.08	0.63 ± 2.54	0.16 ± 1.61
(0.00,0.05)	-0.81 ± 0.36	-0.63 ± 0.41	-0.73 ± 0.27	-2.65 ± 2.27	2.61 ± 2.34	-0.10 ± 1.63
(0.05,0.20)	0.53 ± 0.65	-0.37 ± 0.80	0.17 ± 0.51	0.87 ± 1.98	-1.99 ± 2.36	-0.31 ± 1.51

Table 18: x_F dependence of Physics A_N^B (Blue Beam), A_N^Y (Yellow Beam) and A_N (Combined). The physics asymmetries were obtained by using formula (6) and (7) with A_N (Inclusive)= A_N (Gap4) and A_N (Background)= A_N (Gap3). (-)charge

x_F	$A_N^B(10^{-2})$	$A_N^Y(10^{-2})$	$A_N(10^{-2})$
(-0.20,-0.05)	16.83 ± 6.66	-16.88 ± 6.78	0.27 ± 4.75
(-0.05,0.00)	-1.02 ± 7.02	-0.65 ± 10.55	-0.91 ± 5.84
(0.00,0.05)	6.74 ± 9.43	-11.22 ± 7.92	-3.79 ± 6.06
(0.05,0.20)	0.15 ± 6.03	4.66 ± 7.61	1.89 ± 4.73

6.4.2 (+) charge

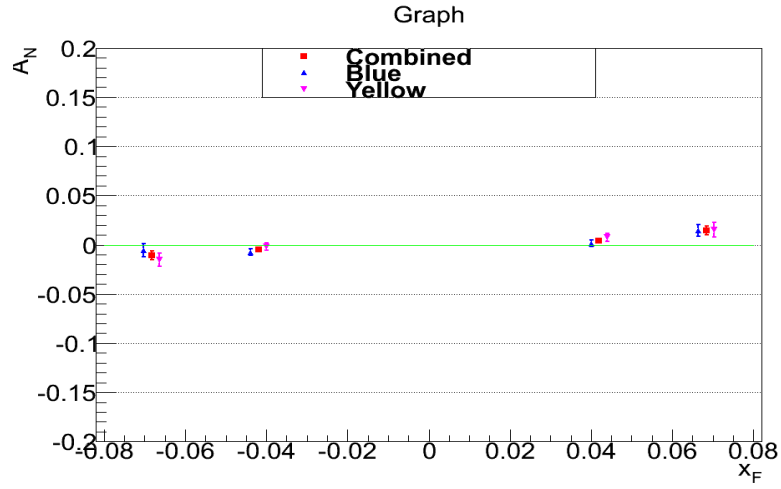


Figure 11: x_F dependence of asymmetries for inclusive muons (Gap4). (+)charge

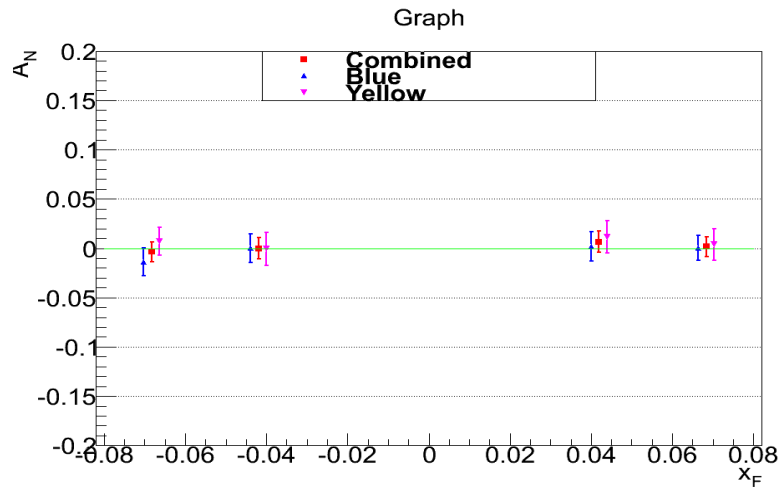


Figure 12: x_F dependence of asymmetries for hadron background (Gap3). (+)charge

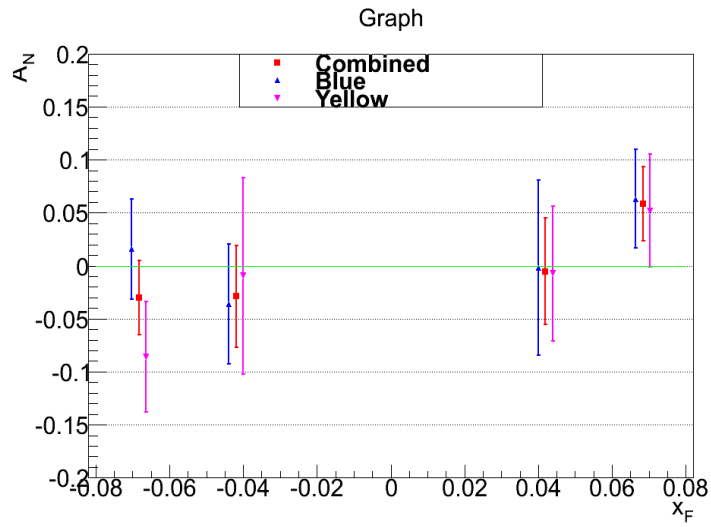


Figure 13: x_F dependence of physics asymmetries, which were obtained by using formula (6) and (7) with $A_N(\text{Inclusive})=A_N(\text{Gap4})$ and $A_N(\text{Background})=A_N(\text{Gap3})$. (+)charge

Table 19: x_F dependence of A_N^B (Blue Beam), A_N^Y (Yellow Beam) and A_N (Combined). (+)charge

x_F	Gap4 (10^{-2})			Gap3 (10^{-2})		
	A_N^B	A_N^Y	A_N	A_N^B	A_N^Y	A_N
(-0.20,-0.05)	-0.57 ± 0.66	-1.53 ± 0.65	-1.06 ± 0.46	-1.37 ± 1.42	0.71 ± 1.44	-0.35 ± 1.01
(-0.05,0.00)	-0.75 ± 0.36	-0.19 ± 0.38	-0.48 ± 0.26	0.01 ± 1.43	-0.05 ± 1.67	-0.02 ± 1.09
(0.00,0.05)	0.13 ± 0.35	0.75 ± 0.40	0.39 ± 0.26	0.21 ± 1.49	1.17 ± 1.62	0.65 ± 1.10
(0.05,0.20)	1.45 ± 0.59	1.51 ± 0.74	1.47 ± 0.46	0.05 ± 1.28	0.39 ± 1.62	0.18 ± 1.01

Table 20: x_F dependence of Physics A_N^B (Blue Beam), A_N^Y (Yellow Beam) and A_N (Combined). The physics asymmetries were obtained by using formula (6) and (7) with A_N (Inclusive)= A_N (Gap4) and A_N (Background)= A_N (Gap3). (+)charge

x_F	$A_N^B(10^{-2})$	$A_N^Y(10^{-2})$	$A_N(10^{-2})$
(-0.20,-0.05)	1.57 ± 4.70	-8.59 ± 5.18	-3.02 ± 3.48
(-0.05,0.00)	-3.62 ± 5.64	-0.94 ± 9.27	-2.90 ± 4.82
(0.00,0.05)	-0.19 ± 8.28	-0.72 ± 6.36	-0.52 ± 5.05
(0.05,0.20)	6.32 ± 4.63	5.19 ± 5.34	5.83 ± 3.50

6.5 Systematic uncertainty

Systematic uncertainty is determined from variation of A_N^{HF} corresponding to upper and lower limit of each background source. Additional systematic uncertainty is from the comparison between two A_N^{HF} calculation methods. The final systematic uncertainty is calculated as a quadratic sum of all systematic uncertainties. The systematic bias has been checked with bunch shuffling technique already in previous analysis note [6]. The sources of systematic uncertainty are listed below, details and tables are listed in Table 21, 22, 23, 24.

δf_h **Fraction of light hadron background**

$\delta A_N^{h \rightarrow \mu}$ **Difference of A_N^h between Gap3 and Gap4**

$\delta A_N^{J/\psi \rightarrow \mu}$ **Uncertainty in $A_N^{J/\psi \rightarrow \mu}$**

δA_N^{method} **Comparison with cosine fit method**

6.5.1 δf_h Fraction of light hadron background

Systematic uncertainty on the fraction of light hadron background (δf_h) is an important source of systematic uncertainty on the A_N^{HF} . The upper and lower limits of A_N^{HF} are calculated by 6 with the upper and lower limits of the fraction of light hadron background ($f_h \pm \delta f_h$).

6.5.2 $\delta A_N^{h \rightarrow \mu}$ Difference in Gap3, Gap4 background asymmetry

The asymmetry of light hadron background at MuID Gap4 (A_N^h) is estimated by using stopped hadrons at MuID Gap3. Since the background tracks at MuID Gap4 include decay muons and punch-through hadrons, the A_N of stopped hadrons can be different from the A_N of decay muons due to decay kinematics. In order to quantify the difference between A_N of tracks at MuID Gap3 and Gap4, a toy simulation using the hadron cocktail simulation and an input truth asymmetry (A_N^{true}) is performed. The A_N^{true} is assumed as $0.02 \times p_T$ at $p_T < 5$ GeV/c and 0.1 at $p_T > 5$ GeV/c based on the most extreme case of A_N^h measured at MuID Gap3 among Figure 3, 6. By comparing the mean value of gap4 and gap3 reconstructed asymmetries in Figure 14, The detailed procedure is following:

1. Generate random spin direction (\uparrow, \downarrow) for all tracks.

2. Apply a weight $(1 \pm A_N^{true} \cdot \cos(\phi_0))$ for each track based on the manually assigned initial asymmetry (A_N^{true}). The sign is determined with the random spin direction in the step 1, and ϕ_0 is the azimuthal angle of track at the generation level.
3. Extract A_N^{reco} of the tracks at MuID Gap3 and Gap4 with the azimuthal angle and momentum information at the reconstruction level.
4. Repeat 10000 times from the step 1 to 3 to obtain smooth distributions of A_N^{reco} .

The largest difference between A_N^{reco} at MuID Gap3 and Gap4 is 0.008 in the entire p_T , so ± 0.008 is assigned to the systematic uncertainty. In case of A_N^h in the x_F binning, the difference of A_N^{reco} at MuID Gap3 and Gap4 is quite small, because only 2 bins are used in x_F . Therefore, the uncertainty on $A_N^h(x_F)$ is negligible.

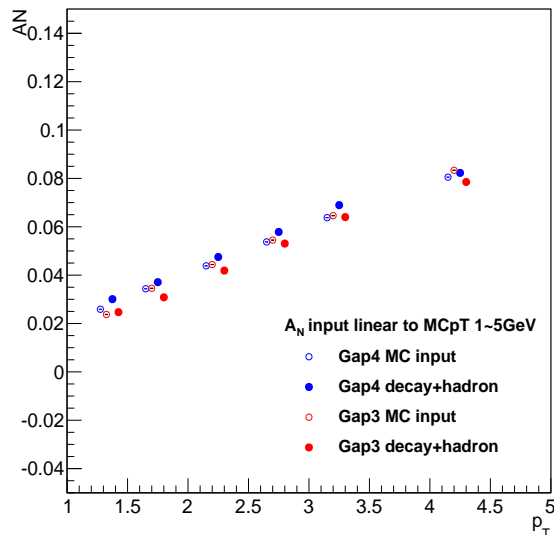


Figure 14: The single Monte Carlo simulation test with $MCp_T \times 2\%$ ($p_T < 5 \text{ GeV}/c$), 10% for $MCp_T > 5 \text{ GeV}/c$ for injected (open circles) and reconstructed (filled circles) asymmetries of gap4(blue) and gap3(red).

6.5.3 $\delta A_N^{J/\psi \rightarrow \mu}$, Uncertainty in $A_N^{J/\psi \rightarrow \mu}$

This has been described in Section 6.2. The systematic uncertainty from $A_N^{J/\psi \rightarrow \mu}$ is determined from $J/\psi \rightarrow \mu$ simulation with the upper and lower limits of $A_N^{J/\psi}$ in [14]. Similar procedure for $\delta A_N^{h \rightarrow \mu}$ was used with Dimuon simulation, while $\delta A_N^{h \rightarrow \mu}$ was made with hadron simulation, $A_N^{J/\psi}(A_N^\mu)$ corresponds to $A_N^{true}(A_N^{reco})$. $A_N^{J/\psi}$ in [14] ($A_N^{J/\psi} = -0.002 \pm 0.026$ in $x_F < 0$, and -0.026 ± 0.026 in $x_F > 0$). The upper and lower limits of A_N^{HF} are calculated by 6 with the upper and lower limits of the $A_N^{J/\psi \rightarrow \mu}$. The initial p_T and rapidity distributions of J/ψ are from [15]. The obtained $A_N^{J/\psi \rightarrow \mu}$ is $-0.002^{+0.018}_{-0.022}$ in $x_F < 0$ and $-0.019^{+0.019}_{-0.025}$ in $x_F > 0$. Figure 15 shows an example of fit of cosine modulation generated by $A_N^{J/\psi}$. Lower side of Figure 16 represents $A_N^{J/\psi \rightarrow \mu}$ distribution by 1000 times of simulation from 6 input $A_N^{J/\psi}$'s(upper side).

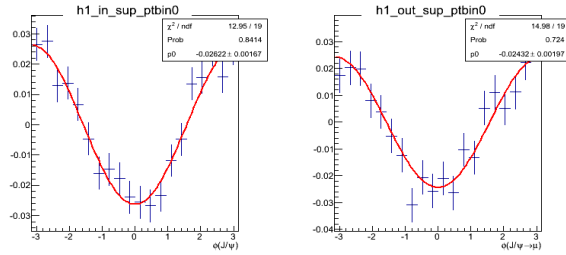


Figure 15: example of fit of cosine modulation induced by $A_N^{J/\psi}$, left is input J/ψ , fit result shows good agreement with input value(-0.026), justifies the procedure and fit. Right side is output muon, different from input $A_N^{J/\psi}$.

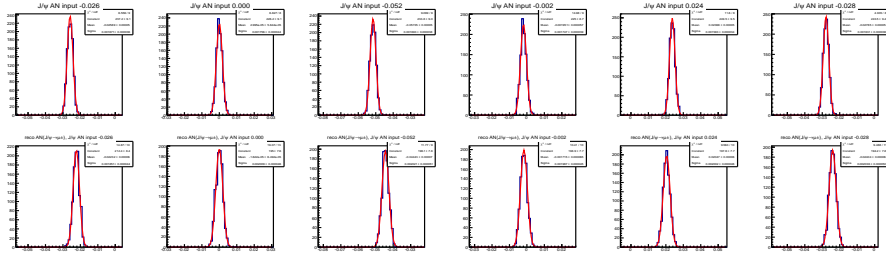


Figure 16: $A_N^{J/\psi \rightarrow \mu}$ distribution(lower side) by 1000 times of simulation from 6 input $A_N^{J/\psi}$ (upper side).

6.5.4 δA_N^{method} , comparison with cosine fit method

The A_N^{incl} results with maximum likelihood method are compared with another method described below. The systematic uncertainty on A_N^{HF} is evaluated by propagating variations of A_N^{incl} and A_N^h between two methods. Since tracks at MuID Gap3 for A_N^h are suffered from large statistical fluctuations, the difference of two methods with inclusive tracks at MuID Gap4 is used for both A_N^{incl} and A_N^h variations. $A_N(\phi)$ of inclusive tracks for each p_T or x_F bin is calculated as,

$$\begin{aligned}
 A_N(\phi) &= \frac{\sigma^{\uparrow\uparrow}(\phi) + \sigma^{\uparrow\downarrow}(\phi) - \sigma^{\downarrow\uparrow}(\phi) - \sigma^{\downarrow\downarrow}(\phi)}{\sigma^{\uparrow\uparrow}(\phi) + \sigma^{\uparrow\downarrow}(\phi) + \sigma^{\downarrow\uparrow}(\phi) + \sigma^{\downarrow\downarrow}(\phi)} \\
 &= \frac{1}{P} \cdot \frac{N^{\uparrow\uparrow}(\phi) + R_1 \cdot N^{\uparrow\downarrow}(\phi) - R_2 \cdot N^{\downarrow\uparrow}(\phi) - R_3 \cdot N^{\downarrow\downarrow}(\phi)}{N^{\uparrow\uparrow}(\phi) + R_1 \cdot N^{\uparrow\downarrow}(\phi) + R_2 \cdot N^{\downarrow\uparrow}(\phi) + R_3 \cdot N^{\downarrow\downarrow}(\phi)},
 \end{aligned} \tag{8}$$

where P is the average beam polarization, $\sigma^{\uparrow\uparrow}$, $\sigma^{\uparrow\downarrow}$, $\sigma^{\downarrow\uparrow}$, and $\sigma^{\downarrow\downarrow}$ are cross section in each polarization combination of two beams, $L^{\uparrow\uparrow}$, $L^{\uparrow\downarrow}$, $L^{\downarrow\uparrow}$, and $L^{\downarrow\downarrow}$ are relative luminosity for each polarization combination, and $R_1 = L^{\uparrow\uparrow}/L^{\uparrow\downarrow}$, $R_2 = L^{\uparrow\uparrow}/L^{\downarrow\uparrow}$, $R_3 = L^{\uparrow\uparrow}/L^{\downarrow\downarrow}$. A_N^{incl} is calculated by fitting $A_N(\phi)$ distribution with a function formed $\pm A_N \cdot \cos(\phi)$, where \pm depends on beam direction. Figure 17, 18, 19, 20 represents cosine fit of Gap4 inclusive tracks. Fit results are compared with Maximum Likelihood method in Figure 21, 22, 23, 24 with χ^2/ndf from the fit results, smaller than 2.

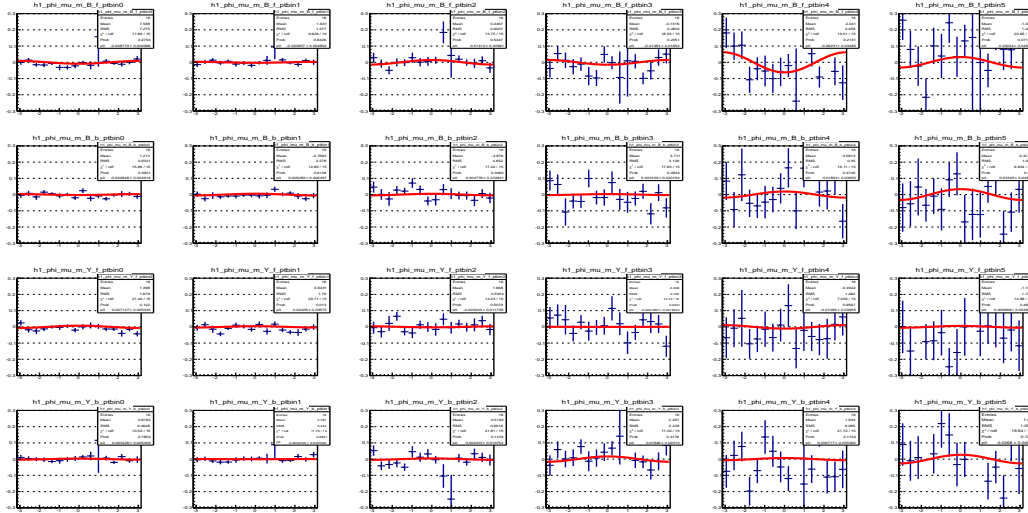


Figure 17: cosine fit result of Gap4 inclusive tracks for 6 p_T bins, (-) charge

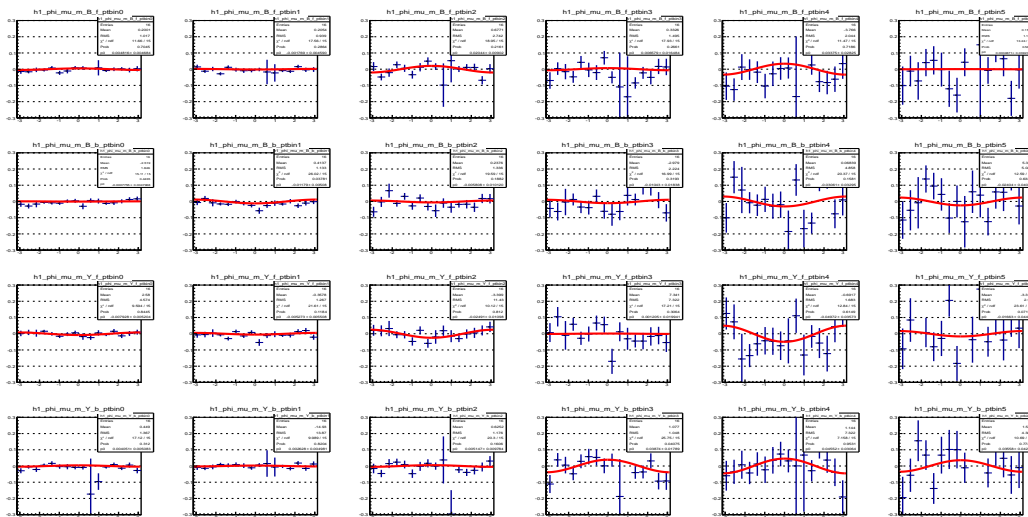


Figure 18: cosine fit result of Gap4 inclusive tracks for 6 p_T bins, (+) charge

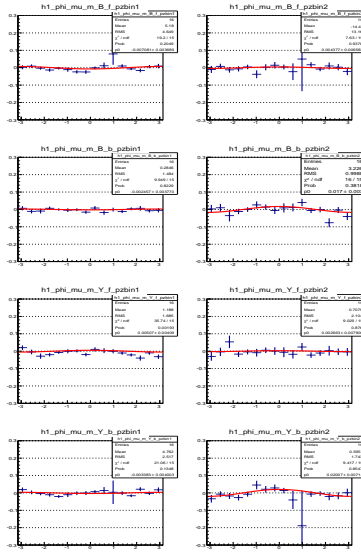


Figure 19: cosine fit result of Gap4 inclusive tracks for 2 p_z bins (4 x_F bins), (-) charge

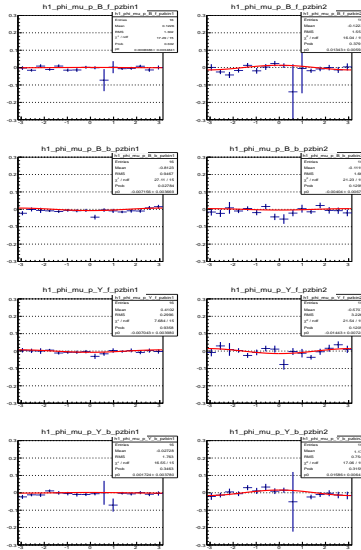


Figure 20: cosine fit result of Gap4 inclusive tracks for 2 p_z bins (4 x_F bins), (+) charge

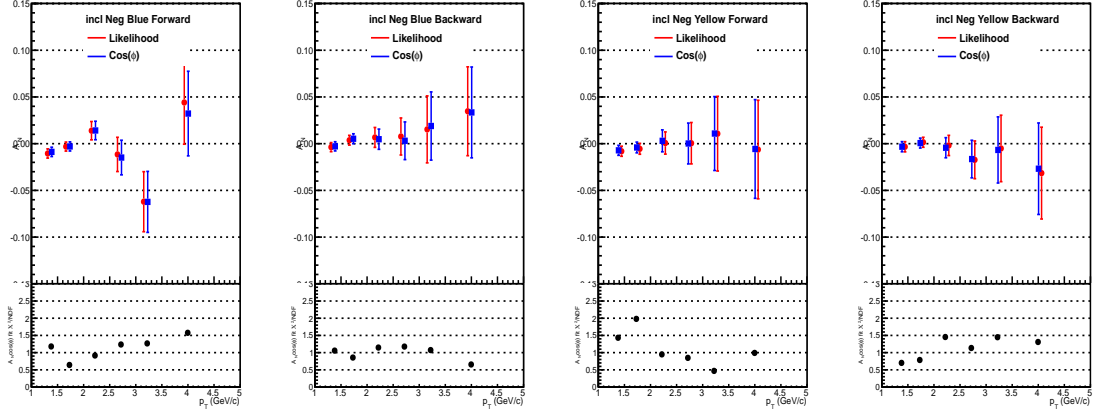


Figure 21: comparison between cosine fit result(blue) and likelihood result (red) of Gap4 inclusive tracks for 6 p_T bins, (-) charge. Lower side represents χ^2/ndf in cosine fit, smaller than 2

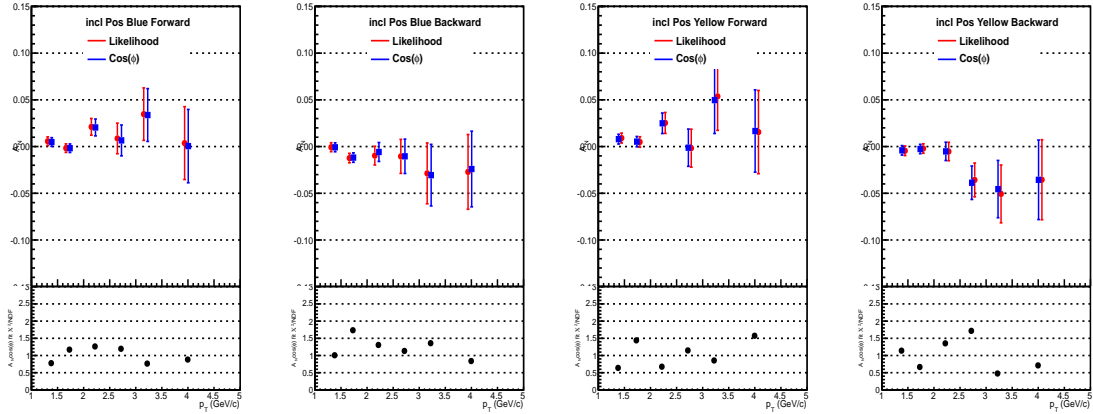


Figure 22: comparison between cosine fit result(blue) and likelihood result (red) of Gap4 inclusive tracks for 6 p_T bins, (+) charge. Lower side represents χ^2/ndf in cosine fit, smaller than 2

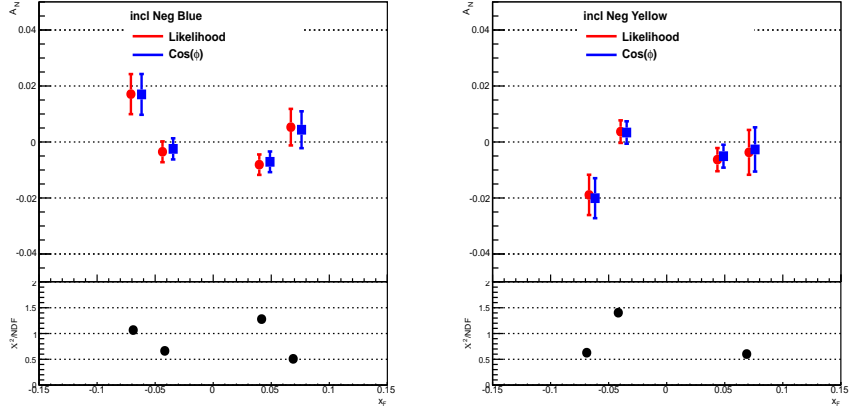


Figure 23: comparison between cosine fit result(blue) and likelihood result (red) of Gap4 inclusive tracks for 4 x_F bins, (-) charge. Lower side represents χ^2/ndf in cosine fit, smaller than 2

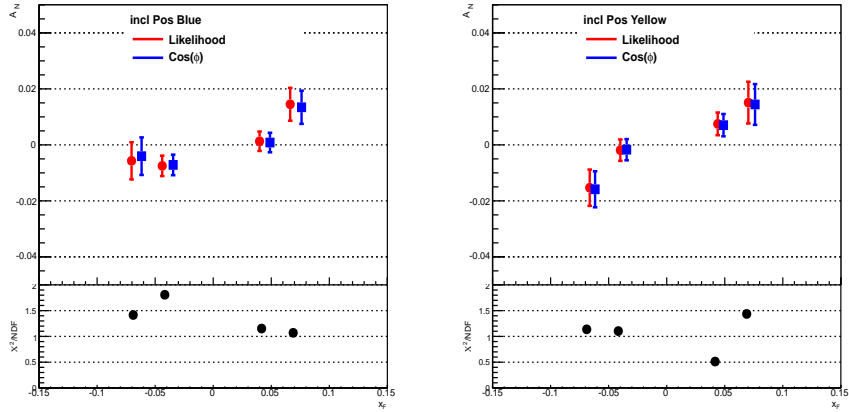


Figure 24: comparison between cosine fit result(blue) and likelihood result (red) of Gap4 inclusive tracks for 4 x_F bins, (+) charge. Lower side represents χ^2/ndf in cosine fit, smaller than 2

Table 21: Sources of $\delta A_N^{syst.}$ for μ^- as a function of p_T .

p_T bin	δf_h	$\delta A_N^{h \rightarrow \mu}$	$\delta A_N^{J/\psi \rightarrow \mu}$	δA_N^{method}
$\delta A_N^{syst.} (10^{-2})$ Forward ($x_F > 0$)				
(1.25,1.50)	+3.56	+2.96	+0.05	+0.81
	-8.96	-2.96	-0.04	-0.81
(1.50,2.00)	+0.29	+2.64	+0.13	+0.37
	-0.06	-2.64	-0.10	-0.37
(2.00,2.50)	+2.37	+2.30	+0.35	+0.59
	-1.20	-2.30	-0.26	-0.59
(2.50,3.00)	+0.43	+1.40	+0.46	+0.69
	-0.40	-1.40	-0.35	-0.69
(3.00,3.50)	+0.75	+1.02	+0.54	+0.05
	-1.06	-1.02	-0.41	-0.05
(3.50,5.00)	+1.78	+0.87	+0.68	+1.85
	-1.38	-0.87	-0.52	-1.85
$\delta A_N^{syst.} (10^{-2})$ Backward ($x_F < 0$)				
(1.25,1.50)	+5.37	+2.95	+0.04	+0.32
	-14.27	-2.95	-0.04	-0.32
(1.50,2.00)	+7.92	+2.67	+0.11	+0.69
	-3.82	-2.67	-0.11	-0.69
(2.00,2.50)	+2.24	+2.26	+0.30	+1.04
	-4.44	-2.26	-0.30	-1.04
(2.50,3.00)	+0.87	+1.39	+0.40	+1.00
	-0.62	-1.39	-0.39	-1.00
(3.00,3.50)	+0.28	+1.01	+0.47	+0.76
	-0.43	-1.01	-0.46	-0.76
(3.50,5.00)	+0.13	+0.87	+0.60	+0.74
	-0.18	-0.87	-0.59	-0.74

Table 22: Sources of $\delta A_N^{syst.}$ for μ^+ as a function of p_T .

p_T bin	δf_h	$\delta A_N^{h \rightarrow \mu}$	$\delta A_N^{J/\psi \rightarrow \mu}$	δA_N^{method}
$\delta A_N^{syst.} (10^{-2})$ Forward ($x_F > 0$)				
(1.25,1.50)	+0.71	+3.37	+0.05	+0.70
	-0.85	-3.37	-0.03	-0.70
(1.50,2.00)	+0.39	+2.55	+0.10	+0.11
	-0.66	-2.55	-0.08	-0.11
(2.00,2.50)	+2.81	+2.28	+0.27	+0.26
	-1.47	-2.28	-0.21	-0.26
(2.50,3.00)	+2.13	+1.67	+0.38	+0.57
	-1.36	-1.67	-0.29	-0.57
(3.00,3.50)	+3.49	+1.33	+0.45	+0.69
	-2.47	-1.33	-0.34	-0.69
(3.50,5.00)	+3.11	+1.31	+0.56	+0.79
	-4.33	-1.31	-0.43	-0.79
$\delta A_N^{syst.} (10^{-2})$ Backward ($x_F < 0$)				
(1.25,1.50)	+0.05	+3.25	+0.04	+0.13
	-0.06	-3.25	-0.04	-0.13
(1.50,2.00)	+0.09	+2.47	+0.09	+0.27
	-0.34	-2.47	-0.08	-0.27
(2.00,2.50)	+0.47	+2.25	+0.24	+1.06
	-1.07	-2.25	-0.23	-1.06
(2.50,3.00)	+2.91	+1.68	+0.34	+0.59
	-4.57	-1.68	-0.33	-0.59
(3.00,3.50)	+2.74	+1.33	+0.40	+1.18
	-4.13	-1.33	-0.39	-1.18
(3.50,5.00)	+0.37	+1.34	+0.50	+0.52
	-0.39	-1.34	-0.49	-0.52

Table 23: Sources of $\delta A_N^{syst.}$ for μ^- as a function of x_F .

x_F bin	δf_h	$\delta A_N^{J/\psi \rightarrow \mu}$	δA_N^{method}
(-0.20,-0.05)	$+0.32 \times 10^{-2}$	$+0.48 \times 10^{-2}$	$+0.30 \times 10^{-2}$
	-1.21×10^{-2}	-0.46×10^{-2}	-0.30×10^{-2}
(-0.05,0.00)	$+0.31 \times 10^{-2}$	$+0.13 \times 10^{-2}$	$+0.45 \times 10^{-2}$
	-0.83×10^{-2}	-0.12×10^{-2}	-0.45×10^{-2}
(0.00,0.05)	$+0.77 \times 10^{-2}$	$+0.14 \times 10^{-2}$	$+0.68 \times 10^{-2}$
	-1.33×10^{-2}	-0.11×10^{-2}	-0.68×10^{-2}
(0.05,0.20)	$+0.54 \times 10^{-2}$	$+0.54 \times 10^{-2}$	$+0.48 \times 10^{-2}$
	-0.38×10^{-2}	-0.41×10^{-2}	-0.48×10^{-2}

Table 24: Sources of $\delta A_N^{syst.}$ for μ^+ as a function of x_F .

x_F bin	δf_h	$\delta A_N^{J/\psi \rightarrow \mu}$	δA_N^{method}
(-0.20,-0.05)	$+0.64 \times 10^{-2}$	$+0.40 \times 10^{-2}$	$+0.57 \times 10^{-2}$
	-1.26×10^{-2}	-0.38×10^{-2}	-0.57×10^{-2}
(-0.05,0.00)	$+0.88 \times 10^{-2}$	$+0.10 \times 10^{-2}$	$+0.17 \times 10^{-2}$
	-2.59×10^{-2}	-0.10×10^{-2}	-0.17×10^{-2}
(0.00,0.05)	$+0.42 \times 10^{-2}$	$+0.11 \times 10^{-2}$	$+0.29 \times 10^{-2}$
	-1.29×10^{-2}	-0.09×10^{-2}	-0.29×10^{-2}
(0.05,0.20)	$+2.25 \times 10^{-2}$	$+0.45 \times 10^{-2}$	$+0.46 \times 10^{-2}$
	-1.21×10^{-2}	-0.34×10^{-2}	-0.46×10^{-2}

7 Simulation to convert theory calculation for A_N of D meson into A_N of muon

7.1 Simulation to convert theory curve for A_N of D meson into A_N of muon in the kinematic region of this measurement

A recent theory incorporating collinear factorization framework shows A_N of D meson (A_N^D), produced from $gg \rightarrow c\bar{c}$ process, which is sensitive to the three-gluon correlation function depending on momentum fraction of gluon (x) [16]. Two models including x or \sqrt{x} dependence in the three-gluon correlation function are introduced to compare their behaviors in small- x region, and the overall A_N^D scale is determined by assuming $|A_N^D| \leq 0.05$ in $|x_F| < 0.1$.

In order to compare with our results (A_N^μ), the decay kinematics and cross section of $D \rightarrow \mu$ from PYTHIA [17] has been used to convert A_N^D into A_N^μ . Theory calculations of x_F and p_T dependent A_N for D^0 , \bar{D}^0 , D^+ , and D^- in $-0.6 < x_F^D < 0.6$ (25 values; 0.05 interval) and $1 < p_T^D < 10$ GeV/ c (10 values; 1,2,3,4,5,6,7,8,9,10) are used as input A_N^D , in Figure 26. After getting smooth curve for 10 p_T values for whole x_F range, $A_N(p_T^D, x_F^D)$ are extrapolated linearly in adjacent p_T values, looked reasonable for all p_T and x_F bins in the region of $|x_F| < 0.2$. A similar procedure described in the systematic uncertainty evaluation for $\delta A_N^{h \rightarrow \mu}$ is used, but the simulation does not have to be multiple times because PYTHIA simulation has enough statistics while hadron simulation is statistically limited. A weight ($1 \pm A_N^D(p_T^D, x_F^D) \cdot \cos(\phi^D)$) is applied for each muon from D meson, and the sign is determined with a random polarization direction (\uparrow, \downarrow). Then, A_N^μ is extracted by fitting asymmetry of two polarization cases with $A_N^\mu \cdot \cos(\phi^\mu)$ in p_T^μ and x_F^μ regions. 9 bins in $0.02 < |x_F^\mu| < 0.1$, 12 bins in $1.0 < p_T^\mu < 5.0$ are used to get smooth curve. $A_N(p_T^\mu, x_F^\mu)$ is rounded to the three decimal and fit error is about 0.001, negligible. Results from the simulation are listed on Table 25,26,27.

Figure 25 shows p_T and $|x_F|$ distributions of D mesons which decay into muons in the kinematic range of this measurement ($1.25 < p_T^\mu < 5.0$ GeV/ c , $0.0 < |x_F^\mu| < 0.2$, and $1.4 < |y^\mu| < 2.0$), and accepted charm hadrons are composed of D^0 (18.7%), \bar{D}^0 (20.3%), D^+ (24.2%), D^- (26.1%), and others (D_s^+ , D_s^- , and baryons). Since $A_N^{D^0}$ and $A_N^{D^+}$ ($A_N^{\bar{D}^0}$ and $A_N^{D^-}$) are very close in both models, the effect of different abundance of D mesons between data and PYTHIA is negligible. In addition, the modification of A_N due to decay kinematics smearing is quite small ($< 5\%$ relative difference between A_N^D and A_N^μ). One notes that muons from charm and bottom are combined

in the data, and the contribution from bottom is about 2% (55%) at $p_T = 1$ GeV/ c (5 GeV/ c) according to the FONLL calculation [9]. Therefore, charm contribution is expect to be dominant except for the last p_T bin of A_N^μ ($3.5 < p_T < 5$ GeV/ c). The converted A_N^μ are shown in Fig. 28, 29, and 30, and both calculations are agreed with the data within the statistical uncertainties. The difference between two models becomes larger as increasing $|x_F|$, but it is hard to distinguish a favored model with the current results in $|x_F| < 0.1$.

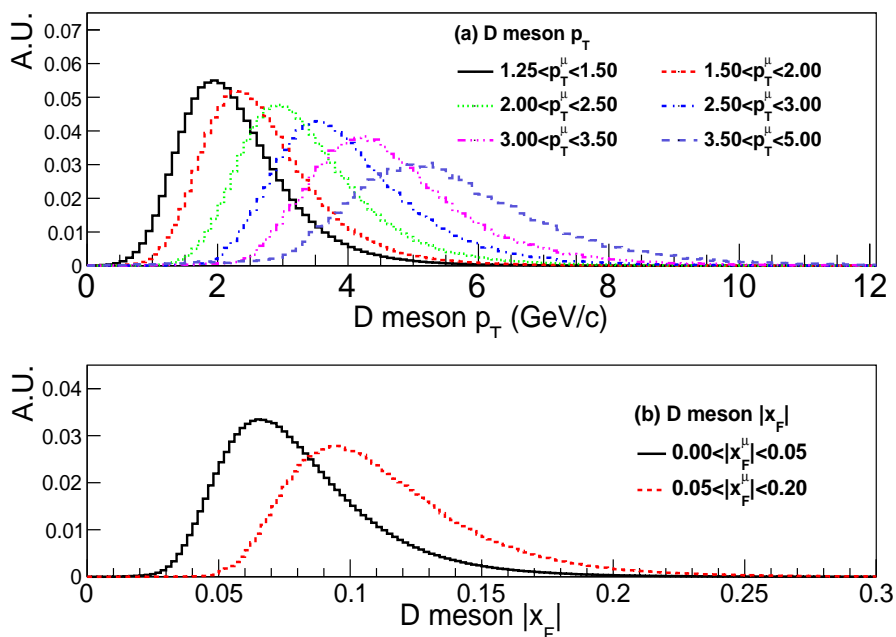


Figure 25: p_T (top) and $|x_F|$ (bottom) distributions of D mesons (D^0 , \bar{D}^0 , D^+ , and D^-) decayed into μ^\pm in $1.25 < p_T^\mu < 5.0$ GeV/ c , $|x_F^\mu| < 0.2$ and $1.4 < |y^\mu| < 2.0$ from PYTHIA. Each distribution is normalized to unity.

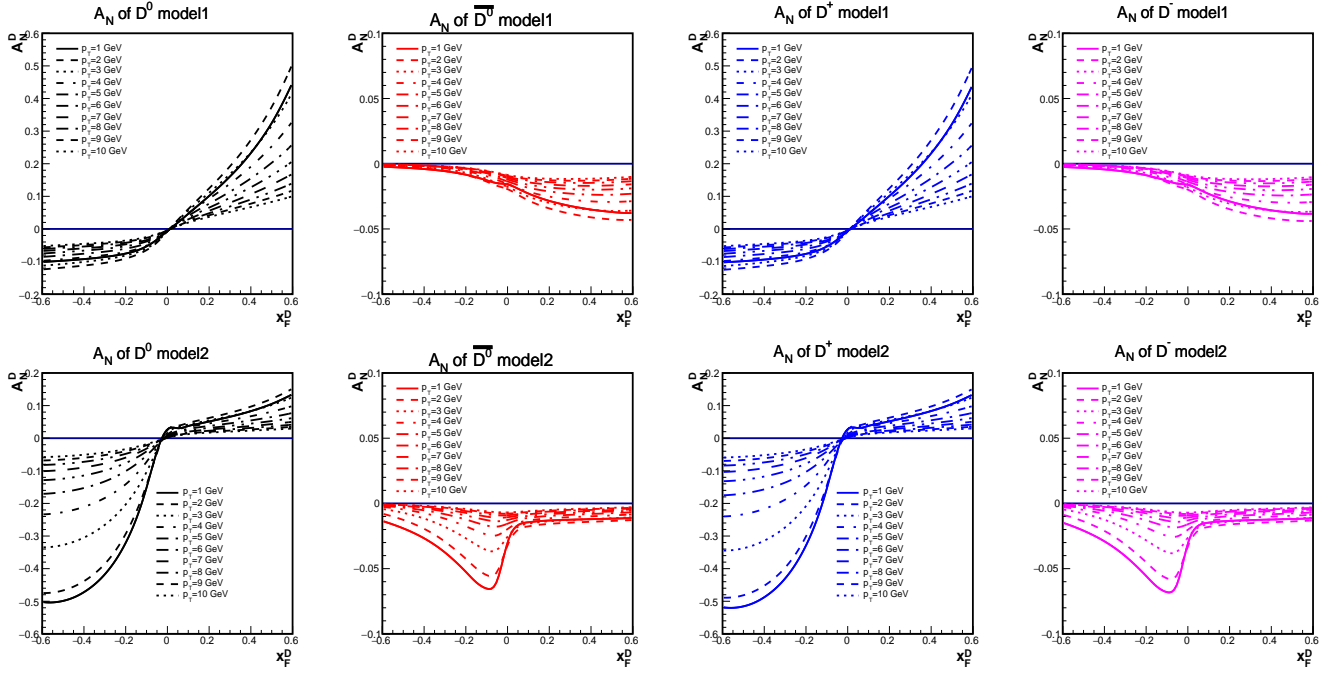


Figure 26: Theory calculation for $A_N^{D^0}$ and $A_N^{D^+}$ $A_N^{\bar{D}^0}$ and $A_N^{D^-}$ as a function of x_F^D ($-0.6 < x_F^D < 0.6$ 25 x_F values; 0.05 interval) for $p_T = 1, 2, 3, 4, 5, 6, 7, 8, 9, 10$ GeV/c [16]

Table 25: Simulation result of A_N of $\mu^- (|x_F| < 0.2)$ as a function of p_T from theory input for D mesons ($\bar{D}^0, D^- \rightarrow \mu^-$).

p_T bin	Forward ($x_F > 0$)		Backward ($x_F < 0$)	
	A_N model 1	A_N model 2	A_N model 1	A_N model 2
(1.00, 1.25)	-0.020	-0.020	-0.017	-0.041
(1.25, 1.50)	-0.022	-0.021	-0.017	-0.040
(1.50, 1.75)	-0.019	-0.018	-0.015	-0.038
(1.75, 2.00)	-0.022	-0.017	-0.016	-0.035
(2.00, 2.25)	-0.022	-0.015	-0.012	-0.035
(2.25, 2.50)	-0.022	-0.015	-0.009	-0.029
(2.50, 2.75)	-0.018	-0.013	-0.011	-0.025
(2.75, 3.00)	-0.019	-0.013	-0.009	-0.023
(3.00, 3.25)	-0.017	-0.011	-0.010	-0.022
(3.25, 3.50)	-0.017	-0.011	-0.009	-0.019
(3.50, 4.00)	-0.017	-0.012	-0.008	-0.015
(4.00, 5.00)	-0.016	-0.007	-0.008	-0.011

Table 26: Simulation result of A_N of $\mu^+ (|x_F| < 0.2)$ as a function of p_T from theory input for D mesons ($D^0, D^+ \rightarrow \mu^+$).

p_T bin	Forward ($x_F > 0$)		Backward ($x_F < 0$)	
	A_N model 1	A_N model 2	A_N model 1	A_N model 2
(1.00, 1.25)	0.010	0.033	-0.023	-0.010
(1.25, 1.50)	0.015	0.032	-0.030	-0.017
(1.50, 1.75)	0.020	0.032	-0.032	-0.025
(1.75, 2.00)	0.024	0.033	-0.035	-0.032
(2.00, 2.25)	0.027	0.032	-0.038	-0.038
(2.25, 2.50)	0.028	0.032	-0.040	-0.045
(2.50, 2.75)	0.029	0.031	-0.039	-0.043
(2.75, 3.00)	0.035	0.031	-0.041	-0.046
(3.00, 3.25)	0.033	0.027	-0.042	-0.045
(3.25, 3.50)	0.034	0.025	-0.041	-0.042
(3.50, 4.00)	0.035	0.026	-0.039	-0.044
(4.00, 5.00)	0.033	0.022	-0.039	-0.041

Table 27: Simulation result of A_N of μ^- (μ^+) in $1.25 < p_T < 5.0$ GeV/ c as a function of x_F from theory input for D mesons ($\bar{D}^0, D^- \rightarrow \mu^-$ or $D^0, D^+ \rightarrow \mu^+$).

x_F bin	$A_N(D^0, D^- \rightarrow \mu^-)$		$A_N(D^0, D^- \rightarrow \mu^+)$	
	model 1	model 2	model 1	model 2
(-0.10, -0.80)	-0.010	-0.022	-0.044	-0.058
(-0.80, -0.60)	-0.013	-0.031	-0.042	-0.051
(-0.60, -0.50)	-0.014	-0.037	-0.037	-0.042
(-0.50, -0.40)	-0.015	-0.039	-0.034	-0.028
(-0.40, -0.30)	-0.016	-0.040	-0.029	-0.016
(-0.30, -0.20)	-0.017	-0.036	-0.025	-0.007
(0.20, 0.30)	-0.021	-0.021	0.011	0.032
(0.30, 0.40)	-0.019	-0.020	0.016	0.032
(0.40, 0.50)	-0.021	-0.019	0.021	0.032
(0.50, 0.60)	-0.023	-0.016	0.026	0.034
(0.60, 0.80)	-0.022	-0.018	0.034	0.033
(0.80, 1.00)	-0.019	-0.013	0.039	0.031

7.2 Additional test with flat A_N input

There are two possible explanations for the difference between $A_N(D \rightarrow \mu)$ and $A_N(D)$. First of all, p_T of D and μ are different, as Figure 25 shows. The asymmetry of muon can be affected by parent D meson. On the other hand, change in azimuthal angle (ϕ) by $D \rightarrow \mu + X$ decay may have an effect on A_N , and there may be more effect as momentum of muon gets lower. Therefore, the flat input $A_N(D)=0.1$ are tested in wide p_T ranges. For $p_T > 1.25$ GeV/ c , output $A_N(D \rightarrow \mu)$ are almost same as $A_N(D \rightarrow \mu)$ for input $A_N(D \rightarrow \mu) = 0.10$. However, $A_N(D \rightarrow \mu)$ is diluted for low p_T ($p_T < 1.0$) in Table 28, Figure 27. $A_N(\mu)$ is smaller for lower $p_T(\mu)$ even though input $A_N(D)$ is fixed as 0.10.

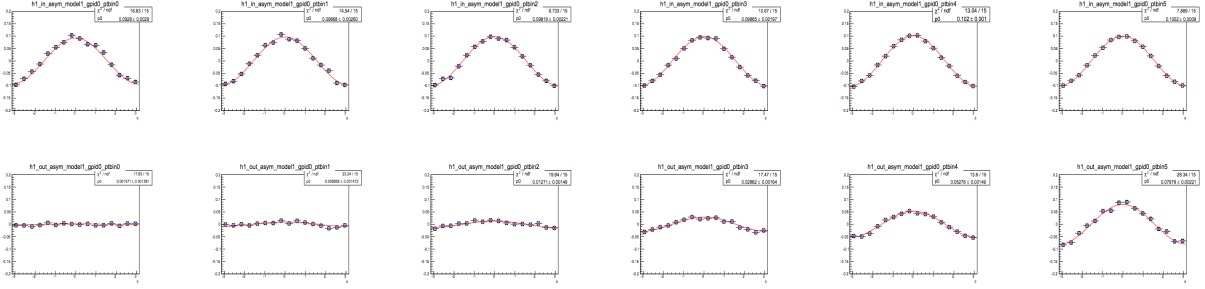


Figure 27: Simulation of $A_N(D \rightarrow \mu)$ from $A_N(D)=0.1$ for low p_T muons (6 bins for $p_T < 1.0$). Upper side is fit result of $A_N(D)$ input and Lower side is fit result of $A_N(D \rightarrow \mu)$.

Table 28: Fit result of cosine modulation for simulation $A_N(D \rightarrow \mu)$ from $A_N(D)=0.1$ for low p_T muons ($p_T < 1.0$ GeV/ c).

muon p_T (GeV/ c)	$A_N(D)$ input	fit result $A_N(D)$	fit result $A_N(\mu)$
(0.0, 0.2)	0.10	0.0928 ± 0.0029	0.0016 ± 0.0014
(0.2, 0.3)	0.10	0.0967 ± 0.0026	0.0088 ± 0.0015
(0.3, 0.4)	0.10	0.0989 ± 0.0022	0.0127 ± 0.0015
(0.4, 0.5)	0.10	0.0987 ± 0.0020	0.0288 ± 0.0016
(0.5, 0.7)	0.10	0.1020 ± 0.0010	0.0528 ± 0.0015
(0.7, 1.0)	0.10	0.1002 ± 0.0009	0.0798 ± 0.0022

8 results

Figure 28, 29, 30 and Table 29, 30, 31, 32 represent the result $A_N^{HF \rightarrow \mu}$ with systematic uncertainty and simulation result from theory ($D \rightarrow \mu$).

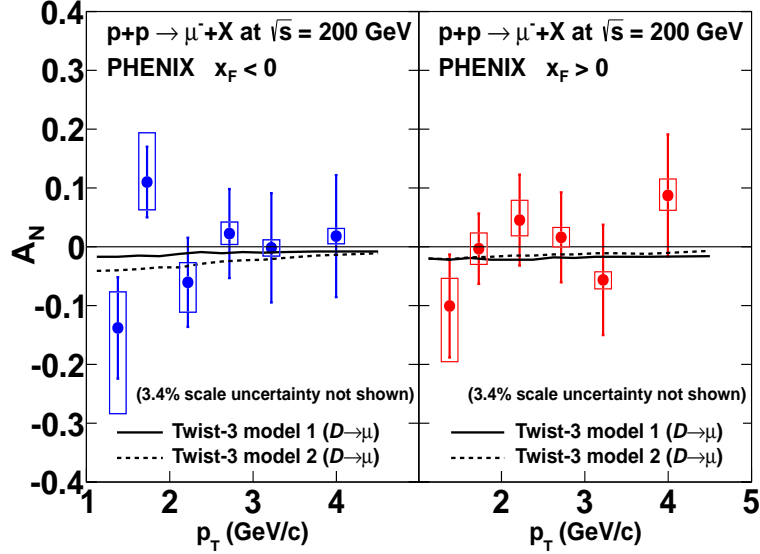


Figure 28: A_N of negatively-charged, heavy-flavor muons as a function of p_T in the backward ($x_F < 0$, left) and forward ($x_F > 0$, right) regions. Vertical bars (boxes) represent statistical (systematic) uncertainties. Solid and dashed lines represent twist-3 model calculations [16].

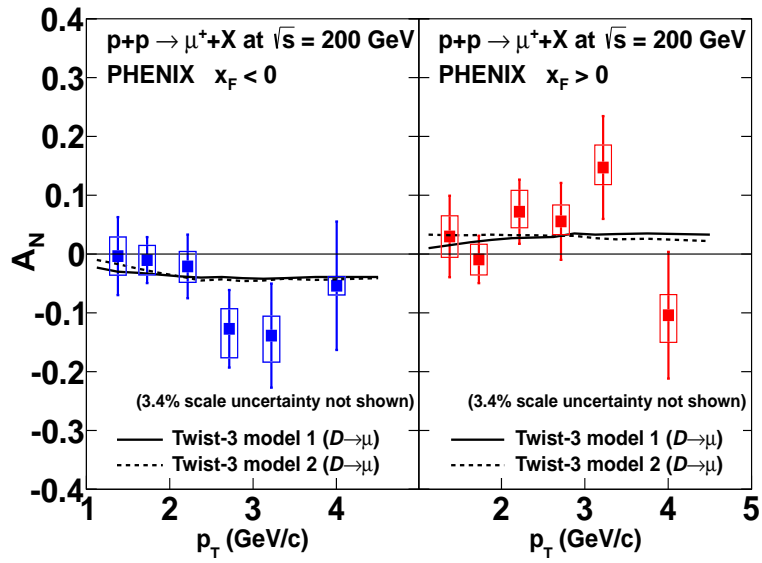


Figure 29: A_N of positively-charged, heavy-flavor muons as a function of p_T in the backward ($x_F < 0$, left) and forward ($x_F > 0$, right) regions. Vertical bars (boxes) represent statistical (systematic) uncertainties. Solid and dashed lines represent twist-3 model calculations [16].

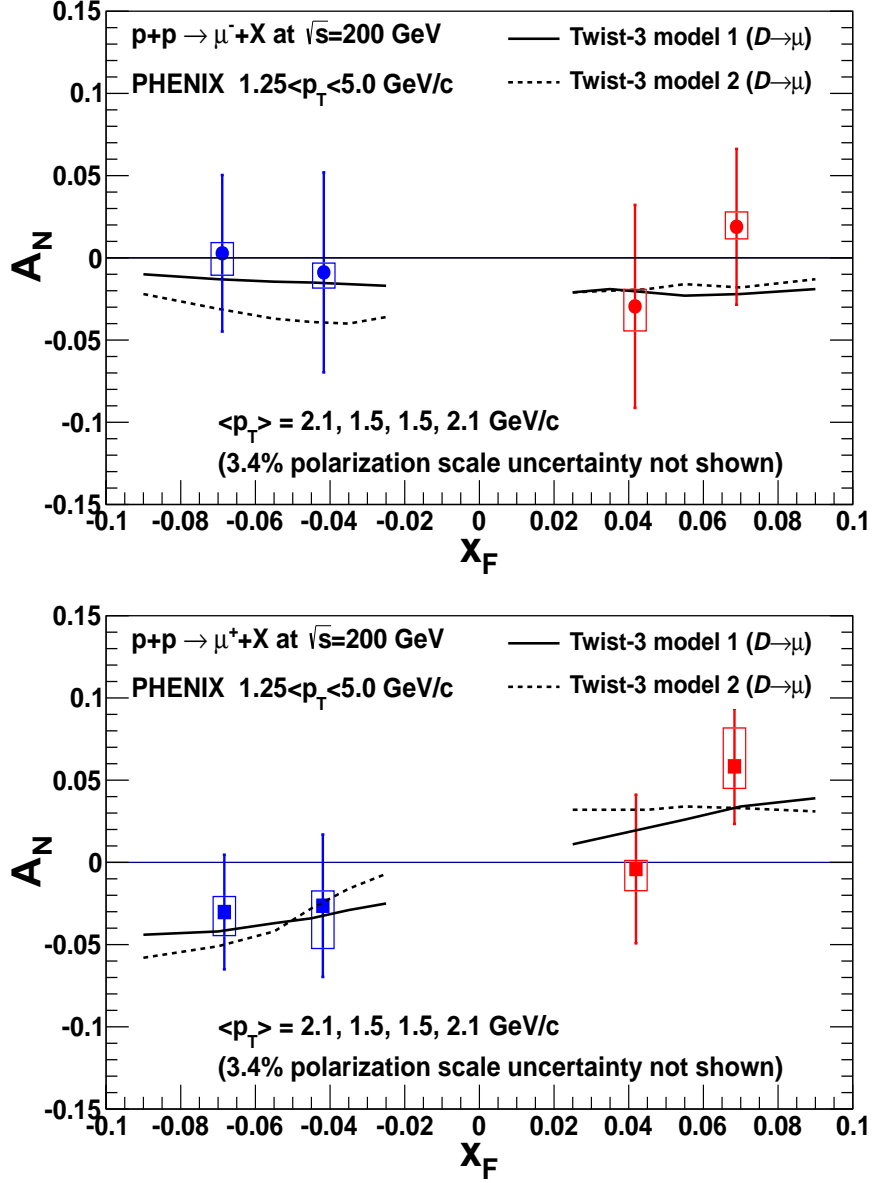


Figure 30: A_N of negatively-charged (top) and positively-charged (bottom), heavy-flavor muons as a function of x_F , where $+x_F$ is along the direction of the polarized proton. Vertical bars (boxes) represent statistical (systematic) uncertainties. Solid and dashed lines represent twist-3 model calculations [16].

Table 29: Data table for A_N of heavy-flavor μ^- as a function of p_T .

p_T bin (GeV/c)	A_N	$\delta A_N^{stat.}$	$\delta A_N^{syst.}$
Forward ($x_F > 0$)			
(1.25, 1.50)	-10.07×10^{-2}	$\pm 8.76 \times 10^{-2}$	$^{+4.49}_{-7.89} \times 10^{-2}$
(1.50, 2.00)	-0.33×10^{-2}	$\pm 5.98 \times 10^{-2}$	$^{+2.68}_{-2.66} \times 10^{-2}$
(2.00, 2.50)	4.54×10^{-2}	$\pm 7.73 \times 10^{-2}$	$^{+3.22}_{-2.65} \times 10^{-2}$
(2.50, 3.00)	1.60×10^{-2}	$\pm 7.65 \times 10^{-2}$	$^{+1.65}_{-1.63} \times 10^{-2}$
(3.00, 3.50)	-5.63×10^{-2}	$\pm 9.38 \times 10^{-2}$	$^{+1.39}_{-1.52} \times 10^{-2}$
(3.50, 5.00)	8.73×10^{-2}	$\pm 10.39 \times 10^{-2}$	$^{+2.70}_{-2.48} \times 10^{-2}$
Backward ($x_F < 0$)			
(1.25, 1.50)	-13.80×10^{-2}	$\pm 8.63 \times 10^{-2}$	$^{+5.80}_{-12.15} \times 10^{-2}$
(1.50, 2.00)	11.01×10^{-2}	$\pm 6.01 \times 10^{-2}$	$^{+7.13}_{-4.45} \times 10^{-2}$
(2.00, 2.50)	-6.05×10^{-2}	$\pm 7.58 \times 10^{-2}$	$^{+3.29}_{-4.73} \times 10^{-2}$
(2.50, 3.00)	2.25×10^{-2}	$\pm 7.57 \times 10^{-2}$	$^{+1.90}_{-1.83} \times 10^{-2}$
(3.00, 3.50)	-0.18×10^{-2}	$\pm 9.29 \times 10^{-2}$	$^{+1.38}_{-1.41} \times 10^{-2}$
(3.50, 5.00)	1.81×10^{-2}	$\pm 10.38 \times 10^{-2}$	$^{+1.30}_{-1.29} \times 10^{-2}$

Table 30: Data table for A_N of heavy-flavor μ^+ as a function of p_T .

p_T bin (GeV/c)	A_N	$\delta A_N^{stat.}$	$\delta A_N^{syst.}$
Forward ($x_F > 0$)			
(1.25, 1.50)	2.99×10^{-2}	$\pm 6.93 \times 10^{-2}$	$^{+3.45}_{-3.51} \times 10^{-2}$
(1.50, 2.00)	-0.92×10^{-2}	$\pm 4.03 \times 10^{-2}$	$^{+2.58}_{-2.64} \times 10^{-2}$
(2.00, 2.50)	7.20×10^{-2}	$\pm 5.46 \times 10^{-2}$	$^{+3.33}_{-2.67} \times 10^{-2}$
(2.50, 3.00)	5.55×10^{-2}	$\pm 6.54 \times 10^{-2}$	$^{+2.57}_{-2.17} \times 10^{-2}$
(3.00, 3.50)	14.71×10^{-2}	$\pm 8.74 \times 10^{-2}$	$^{+3.39}_{-2.71} \times 10^{-2}$
(3.50, 5.00)	-10.40×10^{-2}	$\pm 10.77 \times 10^{-2}$	$^{+3.21}_{-3.99} \times 10^{-2}$
Backward ($x_F < 0$)			
(1.25, 1.50)	-0.35×10^{-2}	$\pm 6.63 \times 10^{-2}$	$^{+3.25}_{-3.25} \times 10^{-2}$
(1.50, 2.00)	-1.03×10^{-2}	$\pm 3.91 \times 10^{-2}$	$^{+2.49}_{-2.50} \times 10^{-2}$
(2.00, 2.50)	-2.10×10^{-2}	$\pm 5.41 \times 10^{-2}$	$^{+2.54}_{-2.70} \times 10^{-2}$
(2.50, 3.00)	-12.71×10^{-2}	$\pm 6.60 \times 10^{-2}$	$^{+3.21}_{-4.33} \times 10^{-2}$
(3.00, 3.50)	-13.87×10^{-2}	$\pm 8.85 \times 10^{-2}$	$^{+3.14}_{-4.12} \times 10^{-2}$
(3.50, 5.00)	-5.39×10^{-2}	$\pm 10.92 \times 10^{-2}$	$^{+1.55}_{-1.55} \times 10^{-2}$

Table 31: Data table for A_N of heavy-flavor μ^- as a function of x_F .

x_F bin	$\langle x_F \rangle$	A_N	$\delta A_N^{stat.}$	$\delta A_N^{syst.}$
(-0.20, -0.05)	-0.07	0.27×10^{-2}	$\pm 4.75 \times 10^{-2}$	$^{+0.68}_{-1.32} \times 10^{-2}$
(-0.05, 0.00)	-0.04	-0.91×10^{-2}	$\pm 5.84 \times 10^{-2}$	$^{+0.55}_{-0.81} \times 10^{-2}$
(0.00, 0.05)	0.04	-3.79×10^{-2}	$\pm 6.06 \times 10^{-2}$	$^{+1.34}_{-2.89} \times 10^{-2}$
(0.05, 0.20)	0.07	1.89×10^{-2}	$\pm 4.73 \times 10^{-2}$	$^{+0.85}_{-0.71} \times 10^{-2}$

Table 32: Data table for A_N of heavy-flavor μ^+ as a function of x_F .

x_F bin	$\langle x_F \rangle$	A_N	$\delta A_N^{stat.}$	$\delta A_N^{syst.}$
(-0.20, -0.05)	-0.07	-3.02×10^{-2}	$\pm 3.48 \times 10^{-2}$	$^{+0.92}_{-1.32} \times 10^{-2}$
(-0.05, 0.00)	-0.04	-2.90×10^{-2}	$\pm 4.82 \times 10^{-2}$	$^{+1.00}_{-2.93} \times 10^{-2}$
(0.00, 0.05)	0.04	-0.52×10^{-2}	$\pm 5.05 \times 10^{-2}$	$^{+0.58}_{-1.50} \times 10^{-2}$
(0.05, 0.20)	0.07	5.83×10^{-2}	$\pm 3.50 \times 10^{-2}$	$^{+2.01}_{-1.25} \times 10^{-2}$

9 Summary

The transverse single spin asymmetries A_N in prompt muons productions (mostly from open heavy flavor decays) are measured as a function of x_F and p_T by using Run12 data. μ^- is studied as well as μ^+ with new background fraction and smaller systematic uncertainty from cross section analysis[9]. There is no clear indication of a non-zero asymmetry in the results, which have relatively large statistical uncertainties. Theoretical calculations of A_N for D -meson production which take into account multigluon correlations are converted into A_N for muons with the help of PYTHIA in order to compare with the data directly. The calculations are in agreement with the data within experimental uncertainties. Future studies with improved statistics, using data taken with the PHENIX detector at RHIC in 2015, could provide constraints on Sivers-like, three-gluon correlation functions.

References

- [1] D.L. Adams et al., Z. Phys. C 56 (1992) 181.
- [2] A. Bravar et al., Phys. Rev. Lett. 77 (1996) 2626.
- [3] J. Adams et al., Phys. Rev. Lett. 92 (2004)171801.
- [4] DIS2006 conference, Brahms preliminary.
- [5] M. Anselmino et al., Phys. Rev. D 70 (2004) 074025.
- [6] PHENIX analysis note 1188.
- [7] PHENIX analysis note 1098.
- [8] PHENIX analysis note 1174.
- [9] PHENIX analysis note 1250.
- [10] PHENIX analysis note 1096.
- [11] PHENIX analysis note 833.
- [12] PHENIX analysis note 696.
- [13] PHENIX analysis note 1073.

- [14] A. Adare et al. (PHENIX Collaboration) Phys. Rev. D 82, 112008 (2010)]
- [15] PHENIX analysis note 1098
- [16] Yuji Koike and Shinsuke Yoshida, Probing the three-gluon correlation functions by the single spin asymmetry in $p^\uparrow + p \rightarrow D + X$ Phys. Rev. D84, 014026 (2011).
- [17] Torbjrn Sjstrand et al. An Introduction to PYTHIA 8.2. Comput. Phys. Commun. 191, 159-177 (2015).

Appendix

Good run list: Good for both north and south arms:

358710 358711 358717 358720 358722 358724 358725 358740 358742 358743
358749 358750 358751 358752 358754 358758 358759 358767 358768 358771
358772 358773 358776 358777 358778 358779 358780 358782 358783 358985
358986 358988 358991 358992 358996 358997 359293 359294 359313 359314
359316 359317 359319 359320 359321 359322 359323 359516 359518 359519
359520 359522 359523 359533 359534 359535 359551 359554 359556 359570
359574 359575 359696 359697 359699 359703 359704 359705 359706 359707
359708 359746 359760 359762 359763 359764 359791 359793 359794 359795
359796 359797 359798 359799 359800 359801 359803 359804 359912 359913
359916 359917 359918 359921 359923 359924 359926 359927 359934 359936
359939 359940 359945 359946 359948 359954 359989 359990 359991 359993
359995 359996 359997 359999 360000 360003 360075 360076 360077 360079
360081 360082 360083 360088 360089 360125 360126 360128 360132 360135
360136 360138 360139 360140 360141 360297 360299 360300 360301 360302
360303 360304 360311 360312 360370 360371 360372 360379 360381 360382
360383 360384 360385 360386 360440 360442 360443 360445 360446 360447
360448 360450 360457 360458 360460 360502 360510 360512 360513 360514
360516 360517 360518 360519 360521 360639 360640 360645 360646 360647
360649 360650 360653 360654 360656 360658 360816 360818 360819 360848
360849 360852 360853 360854 360855 360856 360857 360861 360921 360922
360924 360925 360926 360928 360929 360930 360934 360999 361000 361002
361003 361004 361008 361010 361076 361077 361078 361079 361080 361081
361082 361083 361084 361085 361086 361088 361195 361196 361199 361201
361202 361203 361207 361239 361240 361244 361563 361564 361565 361569
361570 361640 361641 361644 361645 361646 361647 361648 361650 361741
361742 361743 361753 361756 361757 361758 361759 361760 361762 361764
361770 361772 361906 361909 361910 361914 361918 361919 361921 361922
361923 361924 361944 361945 361946 361964 361965 361967 361969 361970
361971 362050 362052 362053 362082 362083 362085 362142 362149 362152
362153 362154 362155 362157 362158 362159 362212 362213 362214 362215
362217 362220 362222 362224 362225 362226 362227 362297 362301 362302
362303 362304 362305 362306 362307 362308 362309 362310 362400 362402
362405 362406 362407 362409 362410 362486 362489 362503 362504 362508
362688 362690 362694 362695 362696 362697 362699 362700 362703 362951